Doctor's thesis FY 2021

東京大学
THE UNIVERSITY OF TOKYO

博士論文（要約）

Optimization of ablation strategy by *in silico* learning for radical treatment of tachyarrhythmia

（頻脈性不整脈の根治に向けた
in silico 学習による焼灼戦略最適化）

Supervisor Ichiro Sakuma, Professor

Department of Precision Engineering, Graduate School of Engineering,
The University of Tokyo
Student ID: 37-197035

瀬野宏

Hiroshi Seno

Table of Content

Table of figures

List of tables

Chapter 1 Background

1.1 Social context of tachyarrhythmia research

Heart is the organ that beats by electrical excitation that propagate throughout the organ. The electrical excitation originates from the sinoatrial node and propagates to the atrioventricular node, hiss bundle, Purkinje fibers, and finally to the entire ventricular muscle (Figure 1.1) [1]. The term “arrhythmia” is used to refer to any disturbance in the normal propagation of electrical excitation, and there are extrasystoles, where the heartbeat becomes irregular, bradyarrhythmias, where the beat slows down, and tachyarrhythmias, where the beat speeds up. Among the above-mentioned arrhythmias, tachyarrhythmia is a disease with high morbidity and lethality, yet no reliable treatment has been established. For this reason, research on tachyarrhythmia is becoming increasingly important. The following are two typical cases of tachyarrhythmia and an overview of them.

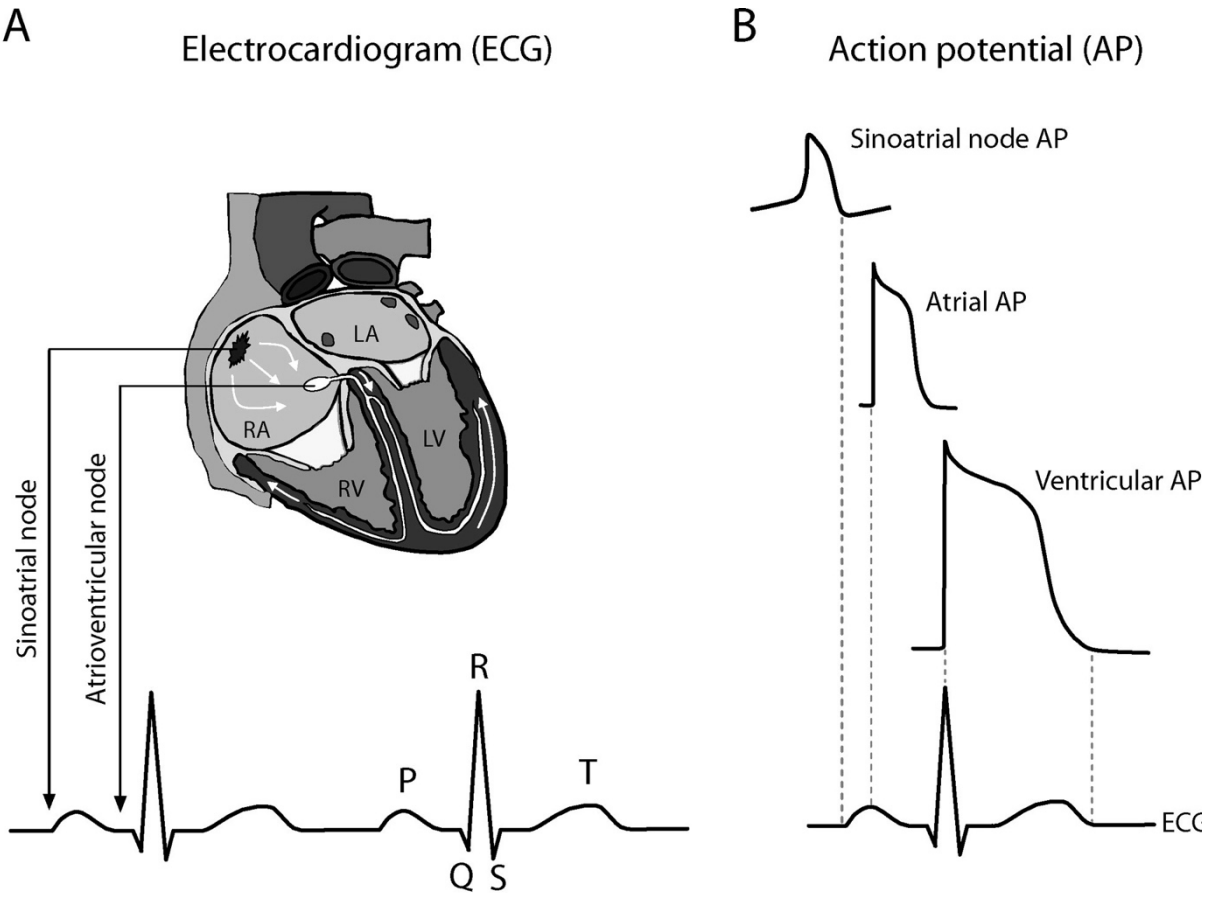

Figure 1.1 Electrical conduction during sinus rhythm [1]

- Ventricular fibrillation

Ventricular fibrillation (VF) is a tachyarrhythmia that occurs in the ventricles. VF causes a rapid decrease in the blood pumping function of the heart, which leads directly to sudden cardiac death. When VF occurs, it is known that the patient generally loses consciousness within a few seconds and the brain and other tissues of the body begin to die within a few minutes. The VF is a cause of sudden cardiac death, accounting for approximately 300,000 to 450,000 deaths annually in the United States alone [2].

- Atrial fibrillation

Atrial fibrillation (AF) is a tachyarrhythmia that occurs in the atria. AF is the most prevalent clinical tachyarrhythmia, and it is estimated that 1–2% of people are affected worldwide [3]. Since AF does not impair the pumping function of the heart, it is not lethal itself, but AF increases the risk of stroke, leading to higher mortality rates in AF patients [4]. Moreover, AF is associated with deterioration of quality of life [5], cognitive impairment [6], and high treatment costs [7]. In addition, AF is a common disease in the elderly, and approximately 10-17% of people aged over 80 years are expected to have AF [8]. Therefore, with the aging of the world population, the number of AF patients has been increasing and is expected to increase further in the future (Figure 1.2) [9].

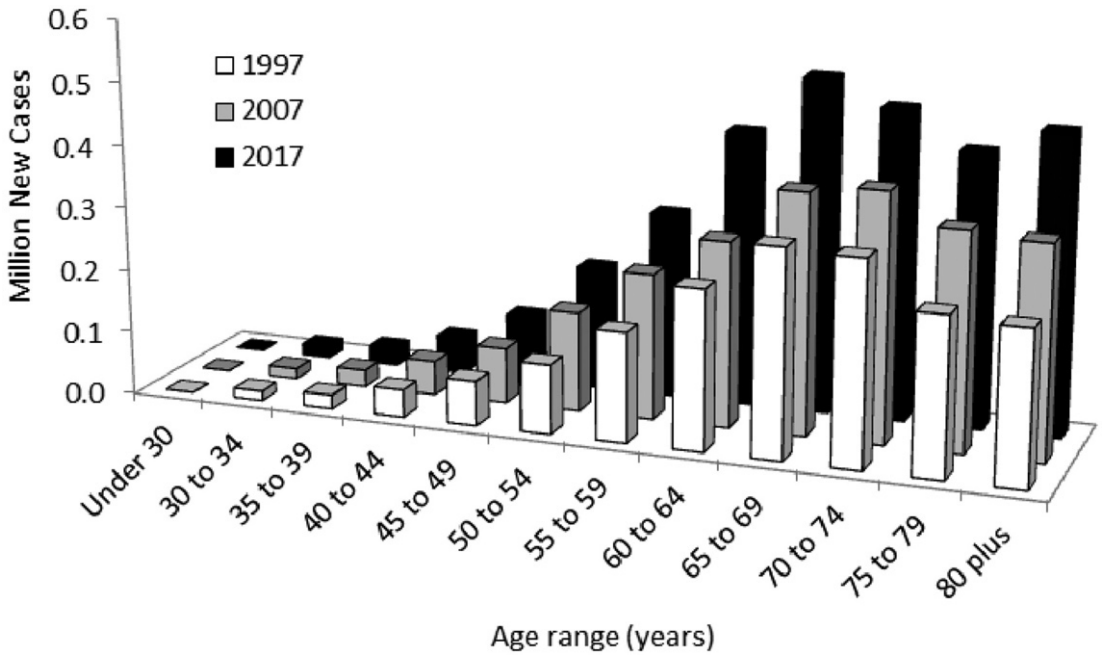

Figure 1.2 Number of AF patients by age group [9]

1.2 Electrophysiology of the heart and mechanism of arrhythmias

1.2.1 Cardiomyocytes and myocardial tissue

Cardiomyocytes are the building blocks of cardiac tissue, and their excitation is mediated by the movement of ions through ion channels, and pumps. These ion channels and pumps are large proteins that penetrate the lipid bilayer of the cell membrane and can selectively move specific ions into and out of the cell through the pores of the proteins [10]. Ion channels and pumps with selective ion permeability generate differences in ion concentrations inside and outside the cell, resulting in the generation of potential differences inside and outside the cell. This potential difference is called the membrane potential.

The potential changes in cardiomyocytes are related to the movement of various ions. Figure 1.3 shows typical membrane potential changes in ventricular cardiomyocytes and sinoatrial node, and the flow of various ions involved in these changes [1]. In the resting state, the ion concentrations inside and outside the cell differ greatly, and the overall membrane potential is negative. The membrane potential in this state is called the resting membrane potential, which is usually about -90 mV. When the surrounding cells are excited or external stimuli occur, the inward sodium ion channel opens and sodium ions flow (I_{Na}) into the cardiomyocytes. This I_{Na} causes a rapid increase in the membrane potential, called depolarization. After depolarization, inward calcium ion channel (I_{CaL}) and outward potassium ion channels (I_{to}, I_{Ks}, I_{Kr}, I_{K1}) follow to open and cancel each other's effects, resulting in a plateau phase in which the membrane potential does not change significantly. After that, the outward delayed rectifier potassium current is activated, and the membrane potential returns to the resting membrane potential. This process is called repolarization. A series of membrane potential changes is called an action potential (AP).

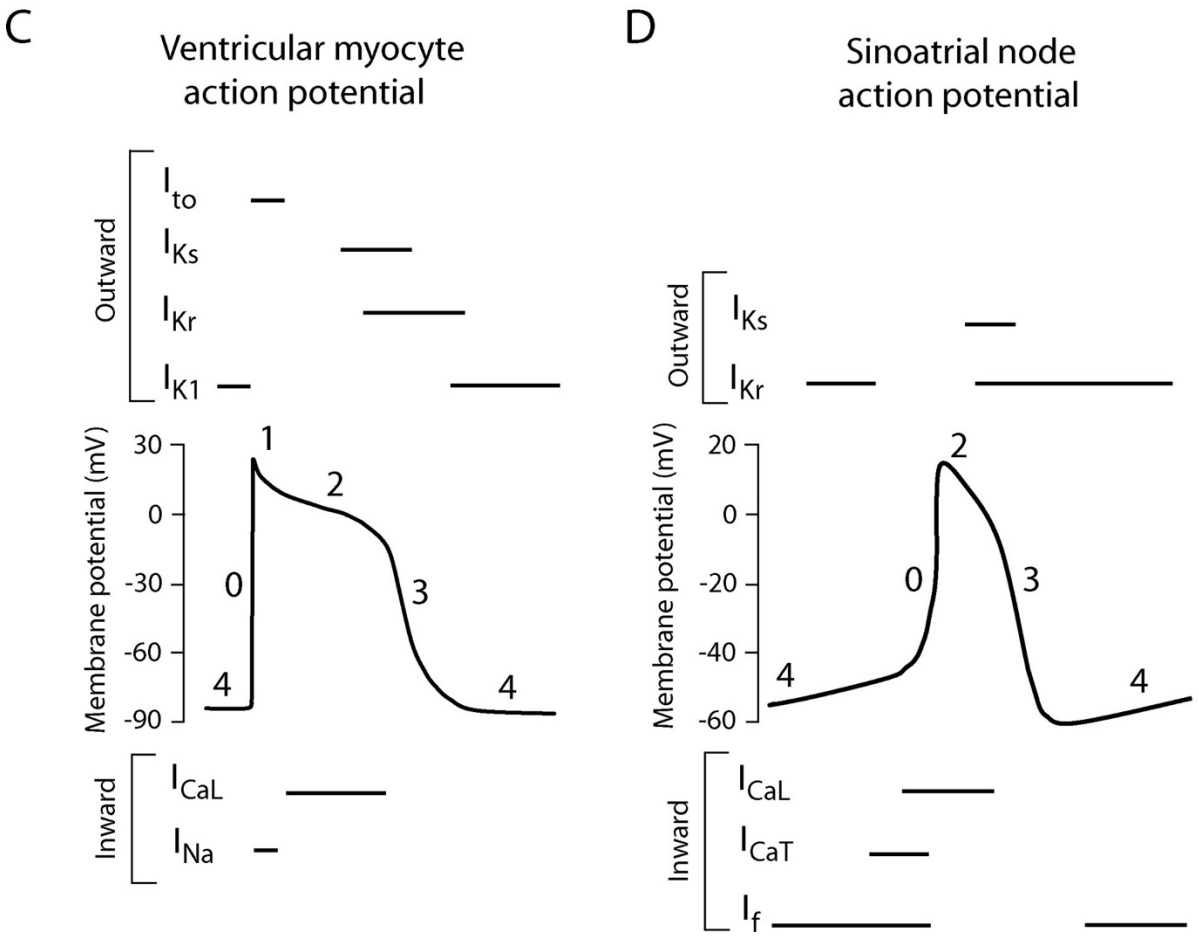

Figure 1.3 Representative cardiac action potential waveforms and ion currents [1]

It is known that cardiomyocytes are not re-excited by new stimuli when the excitation has not cooled down sufficiently, and this characteristic is called the refractory period. This is because, as mentioned above, the I_{Na} responsible for AP depolarization are in the process of being inactivated, and it takes time for them to be reactivated. There are two types of refractory periods: an absolute refractory period (ARP) in which no AP is generated even when a strong stimulus is applied, and a relative refractory period (RRP) in which a different waveform is generated depending on the timing of a stimulus [11]. This refractory period allows excitation to propagate through the heart without backflow and allows the heart to repeatedly contract and relax without keeping contract, even with frequent stimulation.

Myocardial tissue is the physical assembly of cardiomyocytes that are electrically joined together. In myocardial tissue, cardiomyocytes are electrically connected to each other by a channel structure called a gap junction, that allow rapid diffusion of ions. Cardiomyocytes have an elongated structure, and it is known that cardiac fibers are composed of these cardiomyocytes connected via intercalated disks in the longitudinal direction (Figure 1.4) [12]. The gap junction is known to be unevenly distributed in the intercalated disk, and thus myocardial tissues exhibit high conductivity in the direction of the myocardial fibers and are known to have electrical anisotropy.

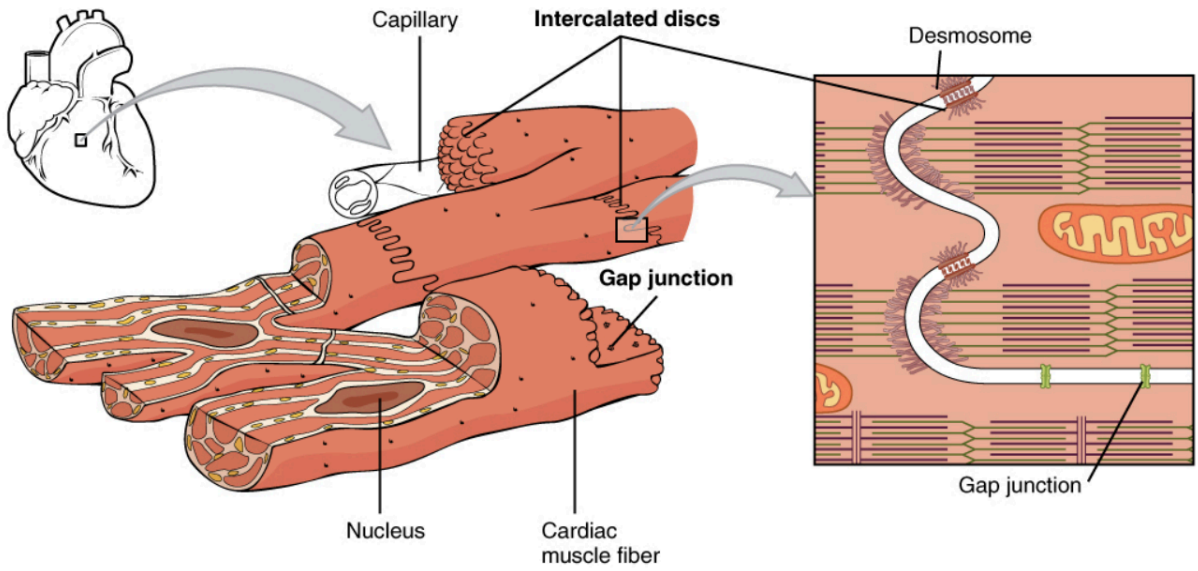

Figure 1.4 Cardiac muscle fibers and gap junctions [12]
Access for free at https://openstax.org/books/anatomy-and-physiology/pages/1-introduction

When a cardiomyocyte in the myocardial tissue is excited, ion influx into the adjacent cardiomyocyte occurs via the gap junction described above, causing a slight increase in the membrane potential of the adjacent cardiomyocyte. This increase triggers the sodium ion current of the adjacent cardiomyocyte to respond, resulting in depolarization. The chain of action potentials in neighboring cells causes excitation waves to propagate throughout the myocardial tissue.

In normal heart organ, only the sinoatrial node functions as a pacemaker, and the other cardiomyocytes only passively propagate action potentials generated by the sinoatrial node. In this way, excitation is propagated in an orderly fashion, and the heart pumps blood as described in Section 1.1.

1.2.2 Mechanism of arrhythmia

The occurrence of arrhythmias is a complex process involving a variety of factors (Figure 1.5) [13]. The genetic factors and environmental stress are thought to cause structural and electrical remodeling of the heart, resulting in arrhythmias. In addition, the occurrence of arrhythmia is thought to spur further remodeling [14], and treatment is needed to break out of this vicious cycle.

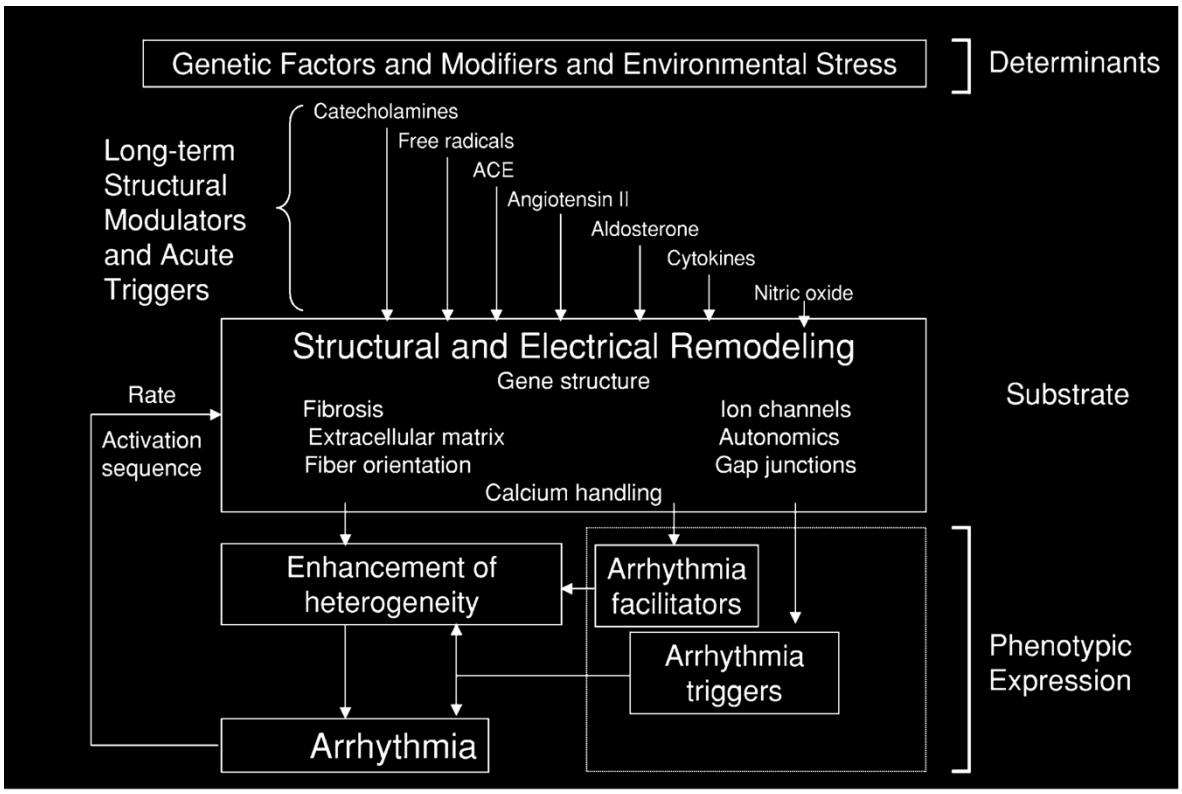

Figure 1.5 Determinants of cardiac arrhythmias [13]

The following is a list of typical arrhythmia phenomena and their mechanisms of occurrence [15].

- Abnormal automaticity

Abnormal automaticity is a condition in which the resting membrane potential of a myocardial cell becomes shallow, from the normal level of -90 mV to around -50 mV, due to factors such as hypokalemia, myocardial ischemia, or degeneration, and is thus susceptible to spontaneous depolarization via calcium ion channels. Normal cardiac excitation is caused by the propagation from the sinoatrial node, but in hearts with abnormal automaticity, spontaneous excitation from sources other than the sinoatrial node also occurs, and this is known to cause tachycardia in general.

- Triggered activity

Triggered activity is a phenomenon in which a spontaneous action potential triggers an abnormal excitation called afterdepolarization, which is followed by depolarization of the cell membrane. The cause is thought to be an abnormality in the calcium ion control mechanism [].

- Reentry

The electrical excitation of normal cardiomyocytes disappears after each cycle. However, under certain conditions, the excitation wave of the heart may return to the area that was once excited and re-excite that area. Such excitation wave is called reentry. Reentries are classified into anatomical reentries mediated by anatomical structures and functional reentries. As typical clinical cases of anatomical reentry, atrioventricular nodal reentrant tachycardia (AVNRT), paroxysmal supra-ventricular tachycardia (PSVT) associated with WPW syndrome are widely known. Functional reentry, on the other hand, has been described using the concept of spiral wave (SW) in a nonlinear excitation medium since the 1990s. In the spiral wave, the excitation front, which is the line of depolarization, curves convexly toward the direction of wave propagation, causing the spiral excitation (Figure 1.6) . The behavior of spiral waves is known to be complex, including meandering, pinning, and splitting.

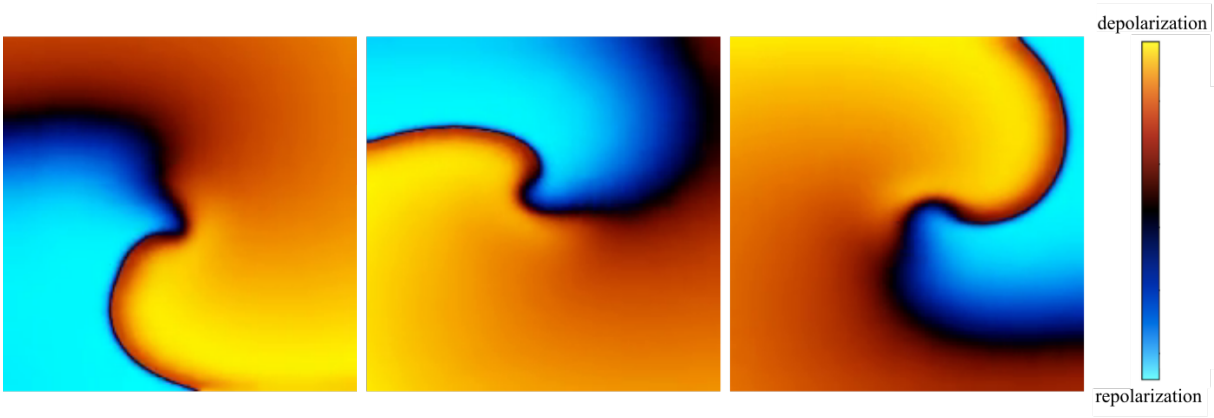

Figure 1.6 Waveform during spiral excitation

1.3 Conventional treatments for tachyarrhythmias

1.3.1 Drug therapy

Antiarrhythmic drugs are used to suppress arrhythmias by acting on cardiac cells electrophysiologically and pharmacologically. The antiarrhythmic agents were categorized according to their individual electrophysiological and pharmacological actions [16], [17].

Drug therapy, which is mostly administered orally, has the advantage of being minimally invasive, but on the other hand, its effects are temporary and cannot fundamentally treat arrhythmia. In addition, some antiarrhythmic drugs have a proarrhythmic side effect due to the nature of its action on ion channels, and analysis of the pharmacological mechanism of effect is being conducted to prevent the induction of arrhythmias by antiarrhythmic drugs [18].

1.3.2 Electrical cardioversion

Electrical cardioversion is also a temporary treatment for tachyarrhythmia in which a strong electrical stimulus is applied to the heart to reset or change the cardiac excitation and restore normal heartbeat. Electrical defibrillation can be divided into two main types.

- Automated External Defibrillator: AED

An AED is a therapeutic device that delivers an electric shock to the heart in ventricular fibrillation (VF) using an external stimulator. The lifesaving rate of patients with ventricular fibrillation decreases with the delay between cardiopulmonary arrest and defibrillation, and AEDs are installed in public and commercial facilities to prepare for emergencies.

- Implantable Cardioverter Defibrillator: ICD

An ICD is a therapeutic device that detects the occurrence of ventricular arrhythmia by means of an electrode implanted in the body, and automatically defibrillates the patient by means of electrical stimulation from a point electrode.

However, some adverse effects also exist with these defibrillation therapies, such as myocardial damages [19], increase in pacing threshold [20], mechanical dysfunction [21], increased risk of sudden cardiac death [22], and mental disorders [23].

1.3.3 Catheter ablation therapy

Ablation surgery is often used in addition to pharmacotherapy, especially for chronic patients with frequent arrhythmias. The ablation surgery attempts to block abnormal excitations that drive arrhythmias by regionally ablating some area of the heart. In this surgery, it is common to insert an ablation catheter through the femoral vein into the cardiac cavity. Although various types of energies are used for ablation. Radiofrequency (RF) ablation, in which cardiac tissue is ablated by Joule heating using radiofrequency current from electrodes, is the most common. In recent years, other types of energies such as freezing and laser is sometime used for some cases.

Catheter ablation is the only therapy with the aim of treating arrhythmias from its source, whereas the other therapies mentioned in Subsection 1.3.1 and 1.3.2 are treatments that temporarily suppress the arrhythmia. Therefore, the ablation therapy has attracted much attention among arrhythmia treatment methods.

However, catheter ablation is not a complete cure for arrhythmia. For example, a survey on the results of catheter ablation for 150 patients of persistent AF reported that arrhythmia-free survival rates after a single catheter ablation procedure were 35.3%±3.9%, 28.0%±3.7%, and 16.8%±3.2% at 1, 2, and 5 years, respectively, and arrhythmia-free survival rates after the multiple ablation procedures (mean 2.1±1.0 procedures) were 89.7%±2.5%, 79.8%±3.4%, and 62.9%±4.5%, at 1, 2, and 5 years, respectively [24]. This study indicates that the treatment effect is not sufficient, and further optimization of catheter ablation therapy is needed for better therapeutic effect of AF.

1.4 Previous related research

1.4.1 Heuristic ablation strategies

In order to improve the therapeutic effect of ablation therapy, various studies have been conducted in the last few decades. There are two main approaches for the treatment using catheter ablation: anatomical approaches [25]–[27] and functional approaches [28]–[31].

- Anatomical approaches

The most common anatomical approach is pulmonary vein isolation (PVI), which targets the pulmonary veins, which is known as the main cause of paroxysmal AF (Figure 1.7) [32]. The PVI is widely accepted as the standard treatment for paroxysmal AF [33], [34]. However, PVI has not been shown to be effective in the treatment of chronic AF. In fact, it is reported that only 60% of patients with chronic AF remained asymptomatic without antiarrhythmic drugs after PVI at 11±8 months of follow-up, and another report said that 5 months after PVI only 22% of patients with chronic AF were free of symptoms [32], [34], [35].

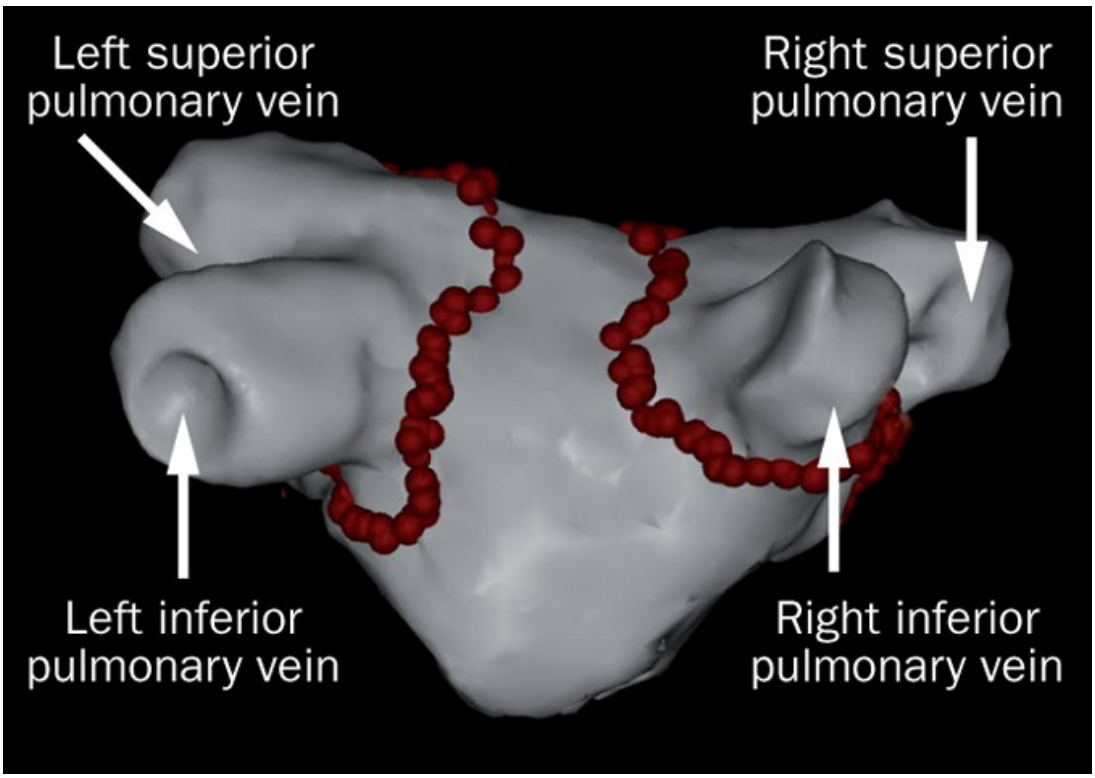

Figure 1.7 Electroanatomical image of PVI surgery (red circles: ablated region) [33]

Other ablation strategies that focus on anatomical structures include linear ablation [36]–[38]. In this approach, linear ablation across the roof of the left atrium, the mitral valve isthmus, and cavotricuspid isthmus is performed [38]. However, in previous research comparing the treatment effect of PVI alone and combination of PVI and linear ablation, it was reported that linear ablation did not significantly improve the treatment effect [39].

- Functional approaches

In recent years, many studies have been conducted to improve the therapeutic efficacy for non-paroxysmal AF, and the functional approach, which identifies the substrate causing abnormal cardiac excitation by measuring extracellular potentials with electrodes and targets it for ablation, has been proposed.

CFAE mapping proposed by Nademanee *et al.* is a typical example of a functional approach [28]. They proposed an ablation strategy that targets complex fractionated atrial electrograms (CFAEs) based on the previous finding that CFAE was observed in functional substrates such as conduction delayed regions in the heart [40]. Ablation of CFAEs was expected to eliminate substrates that drive arrhythmias (Figure 1.8) [28], but a meta-analysis found no significant difference in treatment efficacy between PVI and PVI+CFAE [41].

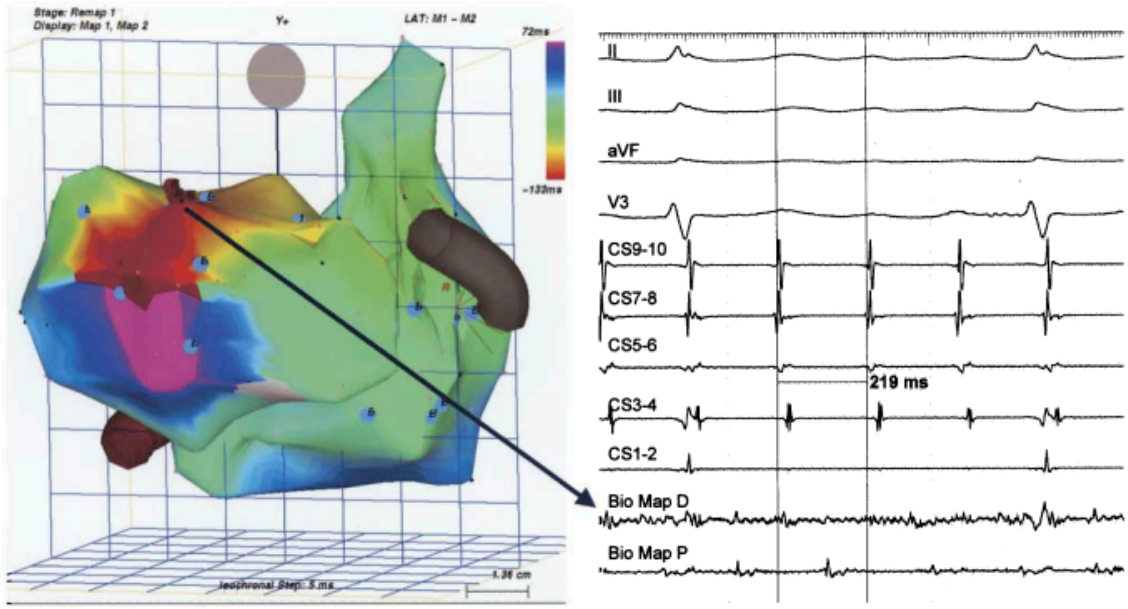

Figure 1.8 Activation map and CFAE [29]

Furthermore, more recently, a method has been proposed to measure spatial potential changes in the heart using a mapping catheter with multiple electrodes and identify the substrate.

The pioneer of ablation based on multiple electrode mapping is FIRM mapping proposed by Narayan et al [29]. In their method, an atrial-sized basket catheter with 64 electrodes was used to measure extracellular potentials at multiple sites throughout the atrial wall, and the excitation pattern of the entire atrium was estimated based on the measured signals (Figure 1.9). They reported that ablation based on the FIRM mapping improved the efficacy of treatment for persistent AF [42]. However, it has been reported that about half of the measuring electrodes used in FIRM mapping were not able to measure interpretable atrial electrograms due to poor contact to the atrial surface [43], and the measurement instability is also responsible for the lack of sufficient therapeutic efficacy in multicenter clinical trials [44].

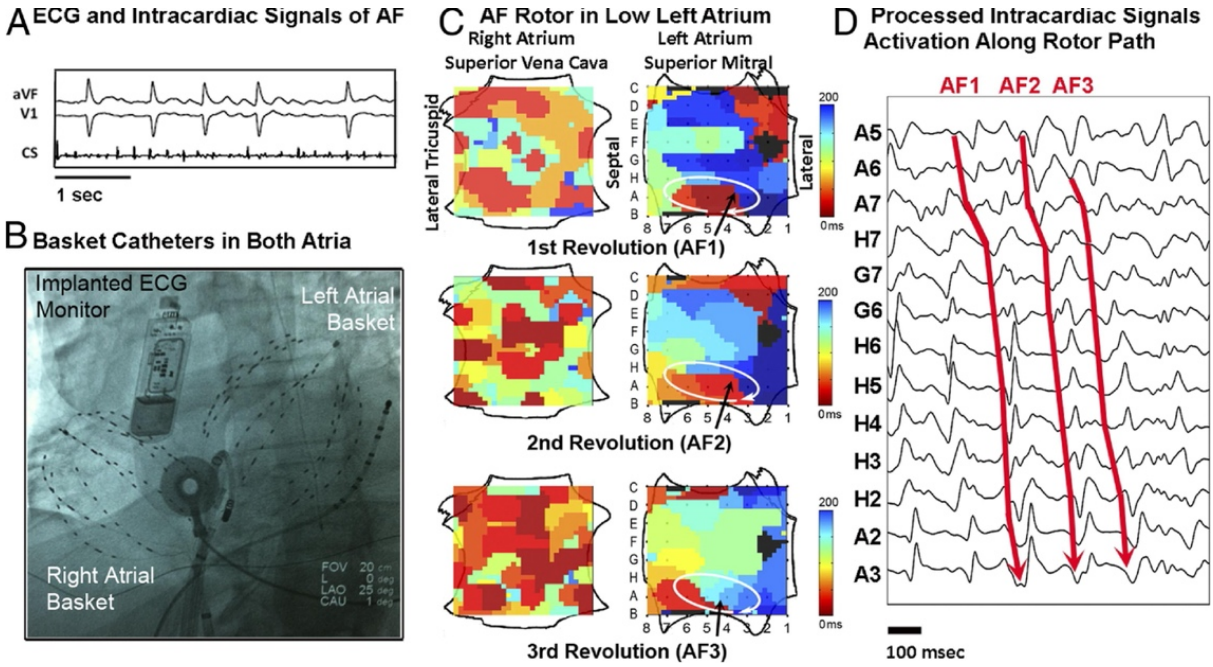

Figure 1.9 Visualization of intracardiac excitation by FIRM mapping [30]

On the other hand, a local mapping-based ablation strategy using high-density electrodes has been proposed in recent years to avoid poor diagnostic accuracy because of poor electrode contact.

A typical example of a local mapping-based ablation strategy is ExTRa Mapping proposed by Ashihara *et al* [31]. This method is expected to improve the contact stability of the electrodes and may allow us to estimate the excitation pattern with higher resolution in the measurement area (Figure 1.10), and in *ex vivo* experiments using rabbit hearts, it has been confirmed that ExTRa Mapping can accurately estimate the direction of propagation of the excitation wavefront and the presence of spiral reentry excitation in the measurement area [45]. It is expected to improve the treatment of chronic AF, but clinical study in a multicenter trial has not yet been reported.

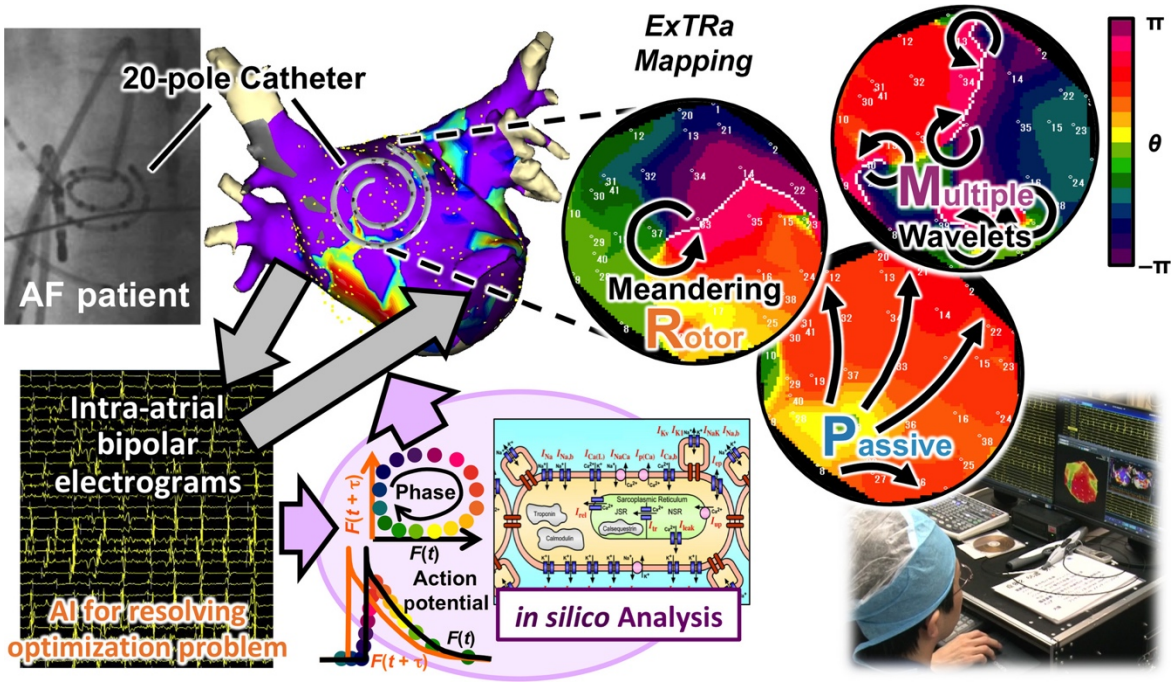

Figure 1.10 ExTRa Mapping [32]

Although various strategies have been proposed as described above, these strategies have not shown sufficient therapeutic efficacy in clinical studies, or their therapeutic efficacy has not been sufficiently confirmed. In addition, they were basically devised subjectively based on the prior knowledge and clinical experience of the proposer, and there is still much discussion about the optimal ablation strategy [46]–[49]. In order to put an end to this discussion, it is necessary to optimize the ablation strategy objectively and quantitatively.

1.4.2 Application of deep neural network

In recent years, deep learning has been applied to a variety of fields. This approach has attracted much attention because of the influence of AlphaGo, which is Go Agent trained in simulator [50]. In optimizing the behavior of a Go agent, Silver *et al.* succeeded in constructing an agent that can beat a human European Go champion by using deep reinforcement learning (Figure 1.11). The example of AlphaGo made a huge impact by showing the possibility of optimization that surpasses human knowledge by deep neural network models instead of imitating human experts.

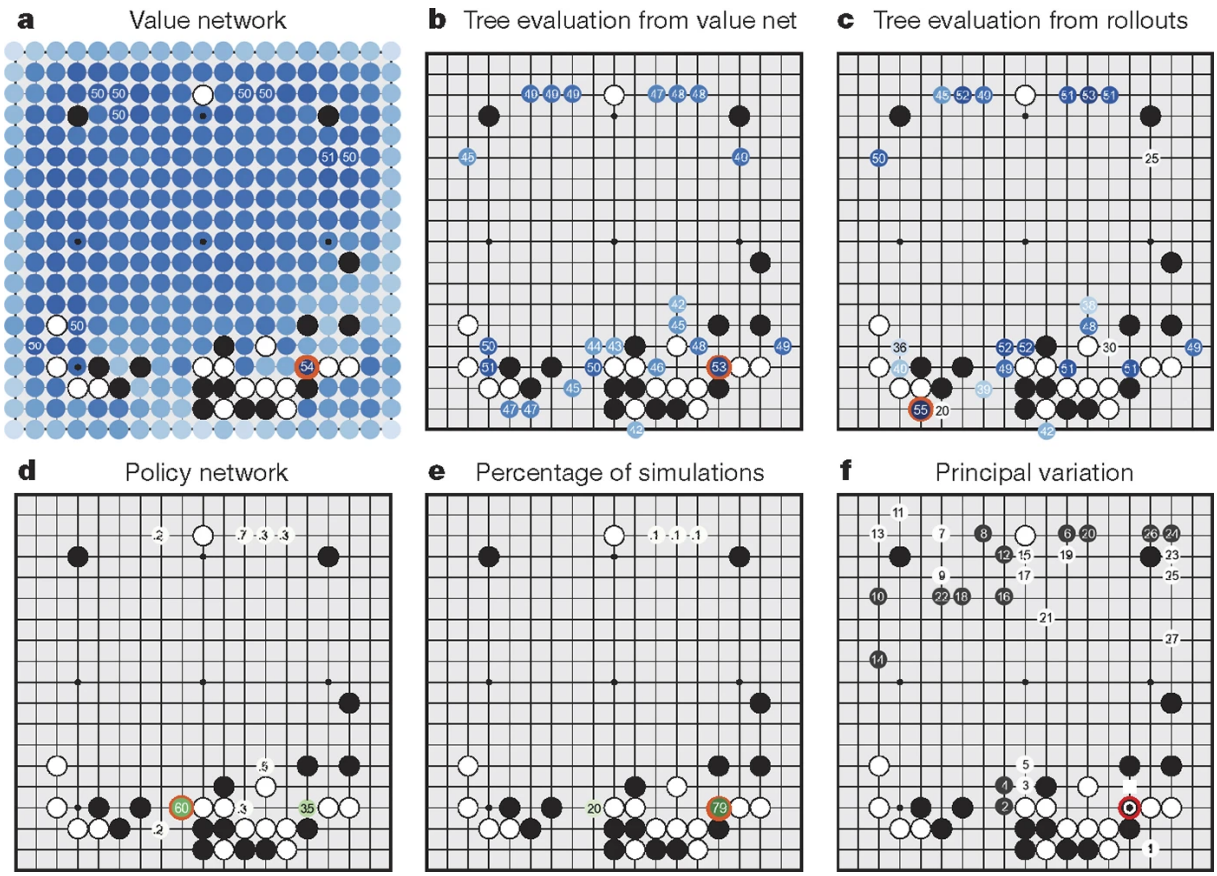

Figure 1.11 How AlphaGo determines its next move [51]

The application of deep neural network has also spread to the medical field, especially for computer-aided diagnosis. For example, there have been many reports of its application to the early diagnosis of cancer [51]–[54], and in the diagnosis of arrhythmia, a model for diagnosing arrhythmia diseases from ECG has been reported [55]. These studies have shown that deep neural network models have the potential to replace the time-consuming diagnoses previously made by doctors and are expected to make a significant contribution to improving efficiency in medicine.

On the other hand, in the medical field, in addition to improving the efficiency of diagnosis, there is also the issue of improving the sophistication of diagnosis, and the application of deep neural network is beginning to expand for this improvement. For example, there is an application of reinforcement learning to control the dosage of sedative drug, and it has been shown that agents trained on pharmacokinetics models can efficiently control the drug dosage [56]. The optimization of the above-mentioned ablation strategy is no exception, and there are previous studies that have attempted to optimize it using deep neural network. For example, Muffoletto *et al.* built a simple simulation model which had the pulmonary veins and fibrotic regions, and then attempted to build a deep neural network model to select an appropriate ablation strategy from three heuristic ablation strategies, using anatomical information such as the location and size of the pulmonary veins and fibrotic regions in the cardiac tissue model as input [57]. Specifically, they first performed three candidate ablation strategies (PVI, fibrosis-targeted ablation, rotor ablation) on each cardiac tissue model in advance and created a dataset of anatomical information of cardiac tissue models and the ablation strategies that had the best probability of stopping spiral excitations (Figure 1.12). Then, the dataset was used for supervised learning to select an appropriate ablation strategy. From this study, they claimed that ablation strategies can be optimized by their proposed method, but their method only selects the better strategy among the three heuristic ablation strategies, and the ablation strategies that cannot be expressed by heuristic ablation are not included in the scope of optimization. Therefore, it cannot be said that this study objectively optimizes the ablation strategy itself.

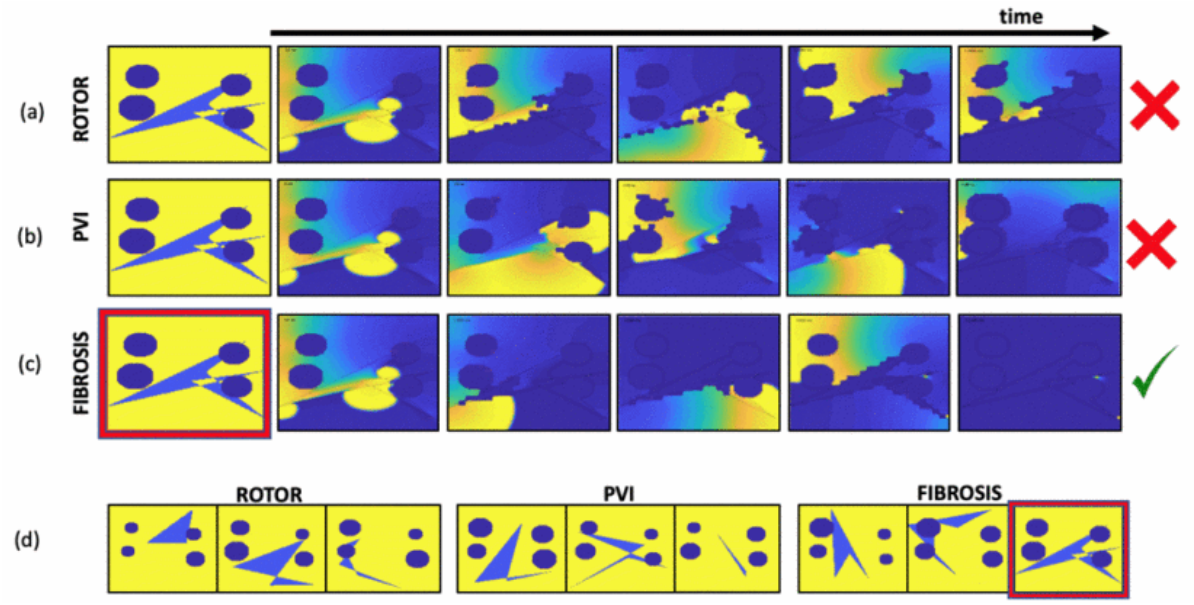

Figure 1.12 Simulations and label assigned for each 2D cardiac tissue model [58]

in silico learning, in which reinforcement learning is performed on a computer simulation to optimize the agent's behavior, as in the case of AlphaGo, is one possible means of objectively optimizing the ablation strategy, but this also has its challenges. The biggest challenge is the high computational cost of the cardiac electrophysiology simulator. As described in Section 1.2, the electrophysiological simulator for cardiac tissue is a kind of reaction-diffusion system in which cardiomyocytes, each of which exhibits nonlinear behavior, are electrically connected and interact with each other. To simulate the phenomena in the reaction-diffusion system, it is necessary to perform iterative calculations with very small time steps to avoid destabilizing the simulation, and to solve differential equations with a large number of variables, which generally increases the computational cost. Therefore, *in silico* learning has not been applied to the control of cardiac tissues because reinforcement learning using a cardiac electrophysiology simulator does not allow for sufficient trial and error. In fact, although Gadaleta et al. have reported that they achieved to control the heartbeat of a single cardiomyocyte by *in silico* reinforcement learning (Figure 1.13) [58], there have been no studies for control of excitation on cardiac tissue, which is a collection of cardiomyocytes.

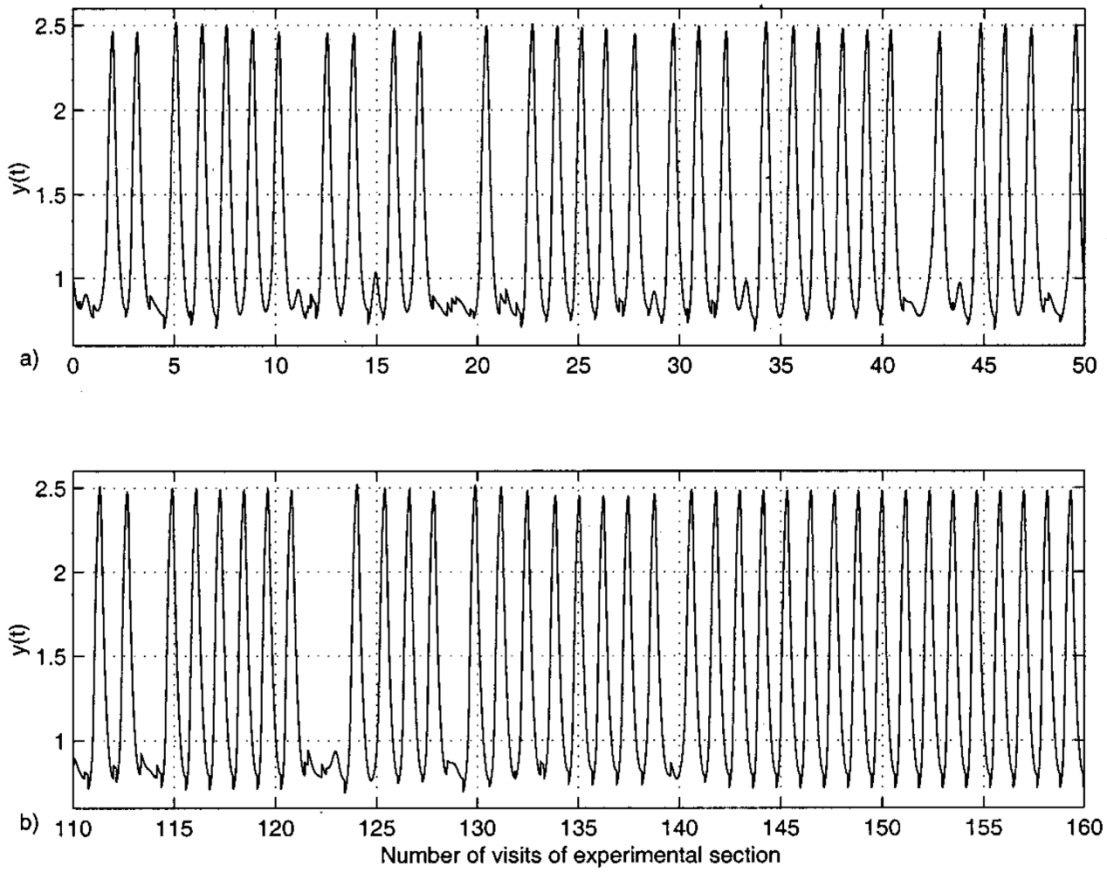

Figure 1.13 Heartbeat control by reinforcement learning [59]

1.5 Objective

In this chapter, an overview of tachyarrhythmia, its current clinical treatment and remaining issues for better treatment have been provided. If the *in silico* learning described above can be applied to the optimization of the ablation strategy, it may be possible to establish an objective and quantitative ablation strategy without being influenced by any electrophysiological prior knowledge that is distinct from the ablation strategies proposed in previous studies, which are based on the prior knowledge and experience of the surgeon. The objective of this study is to optimize the ablation strategy in an objective and quantitative way by applying *in silico* learning to the optimization problem for the better treatment of tachyarrhythmia.

The following thesis is structured as follows (Figure 1.14). Chapter 2 will cover *in silico* learning for optimizing the ablation site. This will be conducted as a proof of concept for optimization of the ablation strategy by *in silico* learning. Chapter 3 will present the construction of an experimental system that enables measurement of membrane potential distribution and implementation of ablation for validation experiment using *in vitro* tissue. In chapter 4, an attempt to stop the spiral excitation in human induced pluripotent stem cell cardiac tissue sheets will be presented. A general discussion, including the overview of the results presented, the significance of this study, limitations, and future works will be covered in chapter 5. Finally, this research will be concluded in chapter 6.

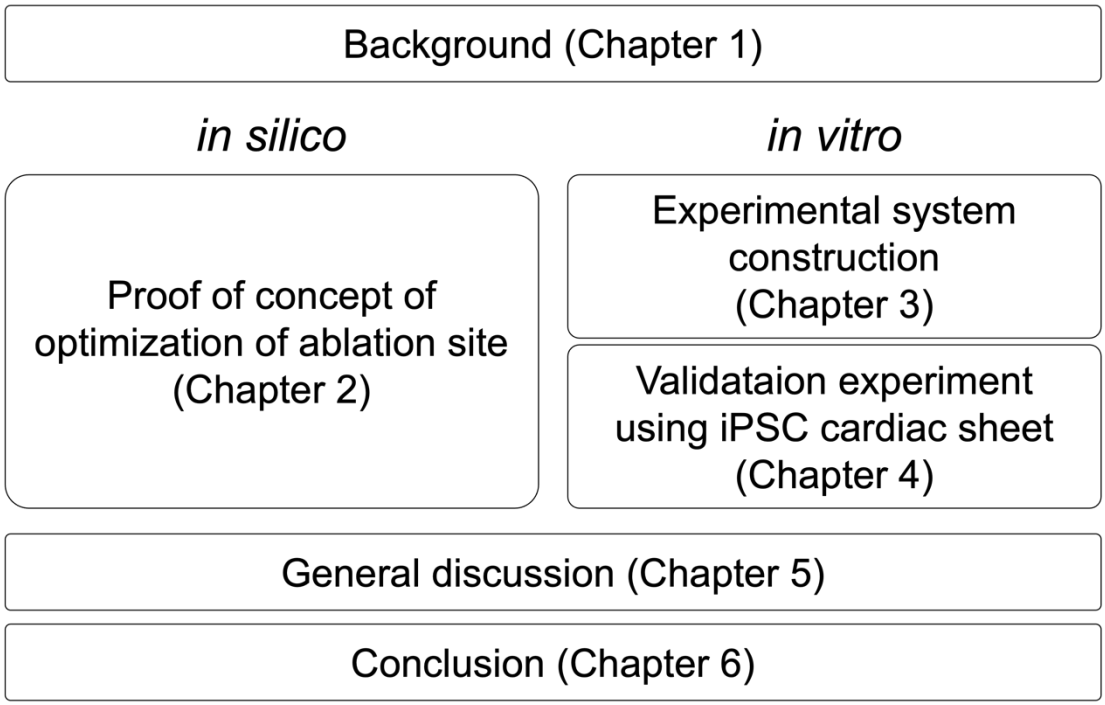

Figure 1.14 Thesis outline

Chapter 2 Optimization of ablation strategy by *in silico* learning

2.1 Objective

In the background chapter, the current status of ablation therapy for tachyarrhythmia was described, and it was confirmed that an appropriate optimization method for ablation strategy has not been proposed, and it is limited to optimization among the ablation strategies that have been proposed so far. If *in silico* learning is applied to the optimization of the ablation strategy, it may be possible to achieve objective and quantitative optimization that is not constrained by conventional methods. However, due to the high computational cost of the cardiac electrophysiological simulator, it may not be possible to obtain a sufficient number of trials for optimization, and the application of *in silico* learning has not been considered so far. In this chapter, a simple two-dimensional cardiac tissue simulation environment was constructed in order to reduce computational cost, and the possibility of optimizing the ablation sites by *in silico* reinforcement learning was investigated on the environment.

2.2 Method

2.2.1 Overview of reinforcement learning scheme

There are various degrees of freedom in the optimization of the ablation strategy: location to be ablated, time-sequence of ablation points, and degree of tissue damage, etc. However, if all these degrees of freedom were to be optimized, the search space would become too large, and the convergence of reinforcement learning might be worsened. Therefore, the optimization target was limited in this case. Among the degrees of freedom in the ablation procedure, the spatial arrangement of the ablation site is considered to be the most dominant in controlling the abnormal excitation in cardiac tissue, and only this ablation pattern was considered for optimization in this study.

Reinforcement learning methods can be broadly classified into value-based algorithms, which estimate the value $Q(s, a)$ of taking action a for state s, and policy-based algorithms, which directly optimize a policy. Value-based algorithms, such as Q-learning and SARSA, have the advantage of being able to optimize for arbitrary policies, but they are known to be unsuitable for optimization of problems with large action spaces. On the other hand, the policy-based algorithm is supposed to be suitable for optimization problems with large action spaces, so the value-based algorithm and the policy-based algorithm need to be chosen appropriately according to the type of optimization problem. If the action space of the ablation pattern is considered, the degree of freedom of the ablation pattern for $w \times h$ candidates is $2^{w \times h}$. For example, if the ablation candidates are 10×10, the action space is about 1.3×10^{30}. Due to the large action space of the ablation pattern, a policy-based algorithm was considered appropriate as the reinforcement learning method to be used in this study.

The policy-based reinforcement learning scheme used in this study is shown in Figure 2.1. First, various spiral reentry excitations were prepared in cardiac simulator and used as an input for a deep neural network-based ablation model (DAM) as shown in red section of Figure 2.1. The DAM was designed to input the movie of the spiral excitation and output preferability of ablation at ablation point candidates. An ablation pattern was generated based on the output of the DAM, and the effect on the spiral excitation by the proposed ablation was evaluated using cardiac simulator (green section of Figure 2.1). Finally, a label was defined based on the simulation results, loss between the DAM output and the label was calculated, and the DAM was updated (blue section of Figure 2.1). By repeating this process of observation, action, and feedback for various spiral excitations, the DAM is expected to learn ablation patterns that effectively stops the spiral excitation.

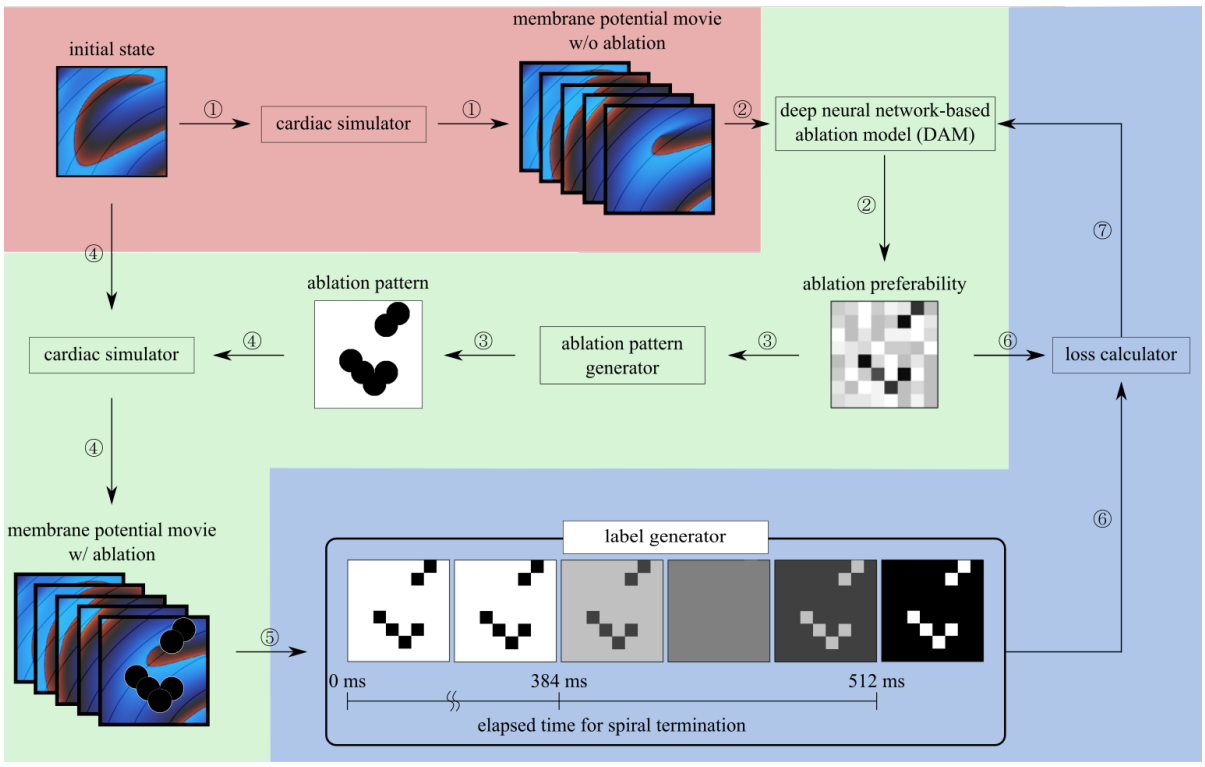

Figure 2.1 Schematic diagram of proposed *in silico* learning scheme.

2.2.2 Components of the proposed learning scheme

2.2.2.1 Cardiac electrophysiological simulator

A cardiac electrophysiological simulator was used as a virtual environment for *in silico* learning. As a cardiac simulator, a mathematical model that simulates the behavior of a single cardiac cell and the excitation of a cardiac tissue in which multiple cardiac cell models are electrically connected is commonly used. Therefore, a cardiac tissue model that simulates the action potentials of cardiac cells and their connections was also used in this study. The details of cardiac cell model and cardiac tissue model used in this study are shown below.

- Cardiac cell model

The basis of the mathematical model of cardiomyocytes is the membrane potential model of the nerve axon of the squid called Hodgkin-Huxley model established in 1952 [59]. Based on this mathematical model, the electrophysiological model of cardiac cells has been continuously improved, and the Luo-Rudy model is representative as a cardiac cell model [60]. Even after the Luo-Rudy model, based on experimental facts, the mathematical modeling for the behavior of ion channels has been improved and cardiomyocyte models for various animal species have been proposed [61]–[64]. In this study, the Courtemanche cardiac cell model was used to simulate the action potential of human atrial cells [61]. The time derivative of the membrane potential is given by Equation 2.1. I_{ion} and I_{st} are the total ion current and stimulus current flowing across the membrane, and C_m is the total membrane capacitance. The ion channels and pumps in the Courtemanche model are shown in Equation 2.2 and Table 2.1. The more details about mathematical modeling in Courtemanche model were described in Appendix A.1.

$$\frac{dV_m}{dt} = \frac{-(I_{ion} + I_{st})}{C_m} \tag{2.1}$$

$$I_{ion} = I_{Na} + I_{K1} + I_{to} + I_{Kur} + I_{Kr} + I_{Ks} + I_{Ca,L} + I_{p,Ca} + I_{NaK} + I_{NaCa} + I_{b,Na} + I_{b,Ca} \tag{2.2}$$

Table 2.1 Ion currents used in Courtemanche model and their definition

Symbol	Definition
I_{Na}	Fast Na^+ Current
I_{K1}	Time-Independent K^+ Current
I_{to}	Transient Outward K^+ Current
I_{Kur}	Ultrarapid Delayed Rectifier K^+ Current
I_{Kr}	Rapid Delayed Outward Rectifier K^+ Current
I_{Ks}	Slow Delayed Outward Rectifier K^+ Current
$I_{Ca,L}$	L-Type Ca^{2+} Current
$I_{p,Ca}$	Ca^{2+} Pump Current
I_{NaK}	Na^+ - K^+ Pump Current
I_{NaCa}	Na^+ / Ca^{2+} Exchanger Current
$I_{b,Na}$	Background Current for Na^+
$I_{b,Ca}$	Background Current for Ca^{2+}
I_{rel}	Ca^{2+} Release Current From Junctional sarcoplasmic reticulum (JSR)
I_{tr}	Transfer Current From Network sarcoplasmic reticulum (NSR) to JSR
I_{up}	Ca^{2+} Uptake Current by the NSR
I_{leak}	Ca^{2+} Leak Current by the NSR

- Cardiac tissue model

When a cardiomyocyte in a cardiac tissue is depolarized, a membrane current is generated, which changes the intracellular and extracellular potential of the surrounding cardiomyocytes. This change in potential further depolarizes the surrounding cardiomyocytes, and propagation of excitation occurs. Cardiac tissue models simulate the interaction between cardiomyocytes in cardiac tissue, and there are two types in cardiac tissue model: bidomain model and monodomain model.

In the Bidomain model, domains with different potentials and conductivities are defined in the inner and outer membranes of cardiomyocytes, respectively, and both the intracellular potential and the extracellular potential changes are calculated numerically (Equation 2.3, 2.4). Here, ϕ_i and ϕ_e are the intracellular and extracellular potentials, $\boldsymbol{\sigma_i}$ and $\boldsymbol{\sigma_e}$ are the intracellular and extracellular conductivity tensor, S_v is the surface-to-volume ratio, and I_i^{ext} and I_e^{ext} are the external stimulus currents inside and outside the cell.

$$\nabla \cdot \boldsymbol{\sigma_i} \nabla \phi_i = S_v I_{ion} - I_i^{ext} \tag{2.3}$$

$$\nabla \cdot \boldsymbol{\sigma_e} \nabla \phi_e = -S_v I_{ion} + I_e^{ext} \tag{2.4}$$

The monodomain model, on the other hand, is a simple model in which the extracellular domain is not defined and only the intracellular domain is calculated. The monodomain model equation is shown in Equation 2.5.

$$\nabla \cdot \boldsymbol{\sigma} \nabla \phi = S_v I_{ion} - I^{ext} \tag{2.5}$$

While the bidomain model is a two-variable equation of ϕ_i and ϕ_e, the monodomain model is a one-variable equation, and it is known that the computational cost can be greatly reduced by the monodomain equation. On the other hand, the monodomain model does not define the extracellular domain, so it is known that it cannot accurately reproduce excitation phenomena such as those caused by extracellular electrical stimulation [65]–[67]. Therefore, the monodomain model was used to reduce computational cost in this study, which is not intended to simulate phenomena that are strongly influenced by extracellular domain, such as extracellular current stimulation. Table 2.2 lists the material constants and the electrical parameters of the monodomain model. The monodomain equation was solved using the finite difference method. If the time step of the finite difference method is too small, the number of iterations increases and the computational cost becomes high, and if it is too large, the computation becomes unstable. In this study, the time step was empirically set to 100 μs to reduce the number of iterations as much as possible without making the calculation unstable. As a boundary condition, the no-flux Neumann boundary condition was used to simulate the electrically insulating region present in the heart. The spatial resolution of the simulator was set to 0.15 mm/pixel, referring to the size of cardiomyocytes, and the membrane potential value of each pixel was sampled at 1 kHz.

Table 2.2 Material constants and electrical parameters of the cardiac tissue model

Parameter (Unit)	Symbol	Value
Membrane capacitance (mF/cm^2)	C_m	1.0
Surface to volume ratio (cm^{-1})	S_v	1400
Conductivity along fiber (mS/cm)	g_{iL}	1.74
Conductivity across fiber (mS/cm)	g_{iT}	0.225

As mentioned in subsection 1.2.2, a cardiac tissue is known to have strong anisotropy depending on the direction of the myocardial fibers, and this anisotropy is one of the factors that complicate cardiac excitation. For this reason, myocardial fiber orientation was introduced into the cardiac tissue simulator by changing the conductivity tensor $\boldsymbol{\sigma}$. The details of the design of fiber orientation are shown in Figure 2.2. The curved fiber orientation was introduced referring to a previous study by Skoubine *et al* [68]. The curve of fiber orientation was set from an ellipse shape with a long axis-short axis ratio of 4:3, centered 15 mm below the simulation area of 60 mm square. On this simulator, the original spiral excitation was induced and used to generate the dataset for *in silico* reinforcement learning.

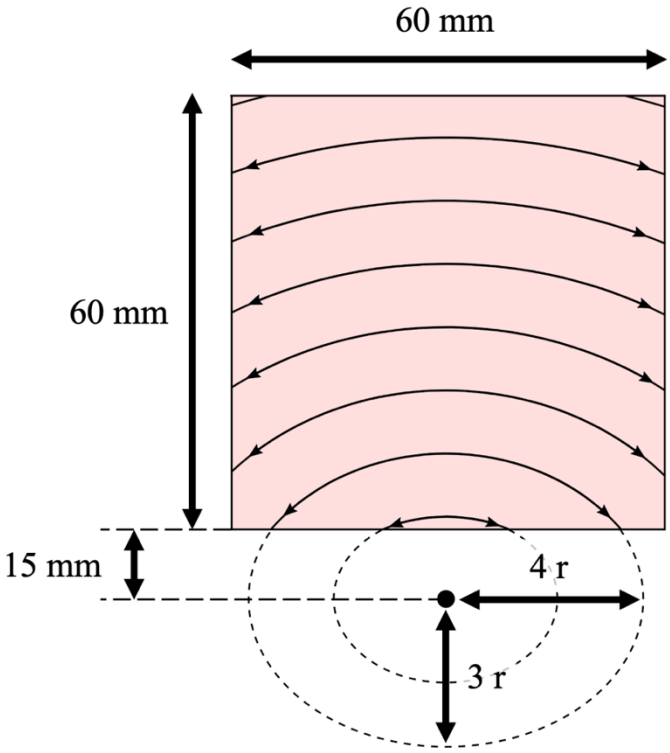

Figure 2.2 Myocardial fiber orientation implemented in cardiac simulator

The dataset was generated by cutting out 38.4 mm square regions from the original spiral excitation generated in the 60 mm square simulation region. By altering the translation, rotation, flipping, and timing of the region to be cut, more diverse data was generated. The time duration of the membrane potential movie input to the deep neural network model must be set appropriately, because too long time duration increases the computational cost, and too short time duration may not provide enough information to understand the excitation state. In this study, the simulation time was set to 512 ms because it includes several spiral turns and is a power of two, which makes easier the convolution operation in the deep neural network model, which will be mentioned later. The generated data, with the exception where spiral excitation spontaneously terminated within 512 ms, were divided into training and test data. Overall, there

were a total of 120 and 360 data sets for training and test purposes, respectively, and 20 of the test samples were used as validation data to check the learning progress.

Ablation in the cardiac tissue model was simulated by setting the conductivity in the ablated area to zero and setting the membrane current of ablated cell to zero. To validate the effect of the proposed ablation, cardiac excitation after the proposed ablation was simulated. The simulation time for training and validation data was set to 512 ms, which is consistent with the time scale of the input movie.

2.2.2.2 Deep neural network model

A deep neural network model was used to determine the location of the ablation from the excitability of the heart. Detailed structure of a deep neural network-based ablation model (DAM) is shown in Figure 2.3. The model was based on 3D U-net, a type of convolutional neural network developed for 3D segmentation tasks [69]. Each box in Figure 2.3 is a shape of the processed data (the number of channels, frames, x pixels, and y pixels) converted by the model. The DAM output the ablation preferability from the membrane potential movie by performing 3D convolution, max pooling, and transformation by activation function. The spatio-temporal resolution of the input membrane potential movie was reduced to 0.60 mm/pixel and 4 ms/frame, respectively, in aim to reduce the computational cost. The resized input was 64 pixels × 64 pixels × 128 frames, which represents 38.4 mm × 38.4 mm × 512 ms cardiac excitation. The output size was 8 pixels × 8 pixels. The ReLU was basically used as the activation function, and the Sigmoid function was used only in the final layer to set the output value from 0 to 1.

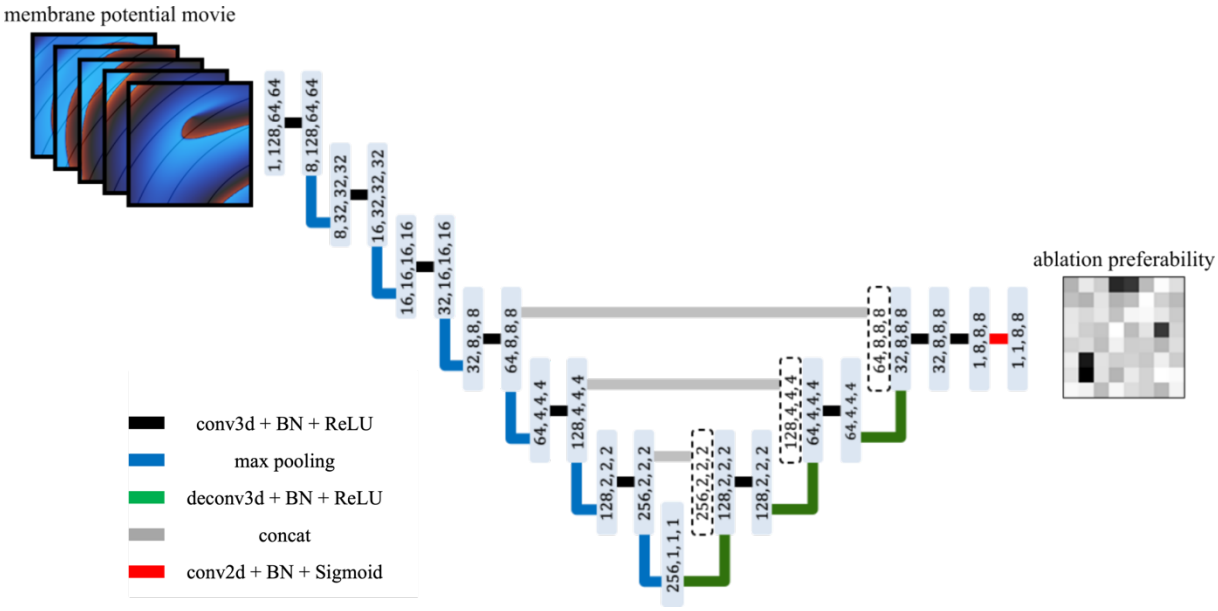

Figure 2.3 Structure of a neural network model

2.2.2.3 Ablation pattern generator

The spatial ablation pattern was generated from the output of the DAM. As mentioned above, the output of the DAM is ranged between 0 and 1 by the sigmoid function, and ablation points were defined as the points where the output value was greater than 0.5. Figure 2.4 shows the design of ablation pattern. The 8 pixels × 8 pixels ablation candidate points were evenly distributed over the entire simulation area, with a spacing of 4.5 mm between each point. The shape of the ablation area from each point was circular in consideration of the thermal diffusion that occurs during ablation. To ensure that adjacent ablations were spatially contiguous, the size of each ablation was 9 mm in diameter, twice the distance between ablation points.

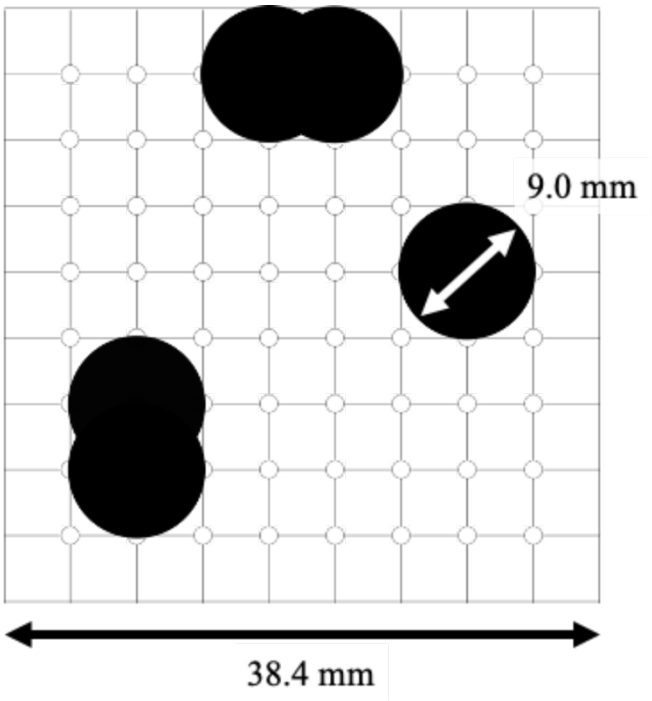

Figure 2.4 Details of ablation pattern design

2.2.2.4 Label generator

In order to learn effective ablation sites, it is necessary to design reward function to reward ablations that can stop the spiral excitation effectively and do not reward or punish ablations that fails. In this study, labels were defined to be compared with the output of the DAM based on the time taken to stop the spiral excitation. Figure 2.5 shows how the labels were defined. The time-sequence of the membrane potential after the proposed ablation by DAM was used to judge the termination of spiral excitations, and the timing of termination was defined as the time point at which the maximum membrane potential value in simulation area fell below -40 mV. If the spiral excitation was terminated by the proposed ablation within 384 ms, which accounts for 75% of the simulated time, the ablation points obtained by binarizing the output of the DAM were defined as the label. On the other hand, if the proposed ablation failed to terminate spiral

excitation within 512 ms, the proposed ablation site was inverted and defined as the label. If the spiral excitation was terminated between 384 ms and 512 ms, a label that changed continuously from the proposed ablation points to the inverted ablation points was defined depending on the termination time. By setting labels in this way, when the DAM output is compared with the labels, it is expected that the loss will be smaller for ablations that successfully stops the spiral excitation and larger for ablations that fails to stop, allowing trial and error for appropriate ablation sites.

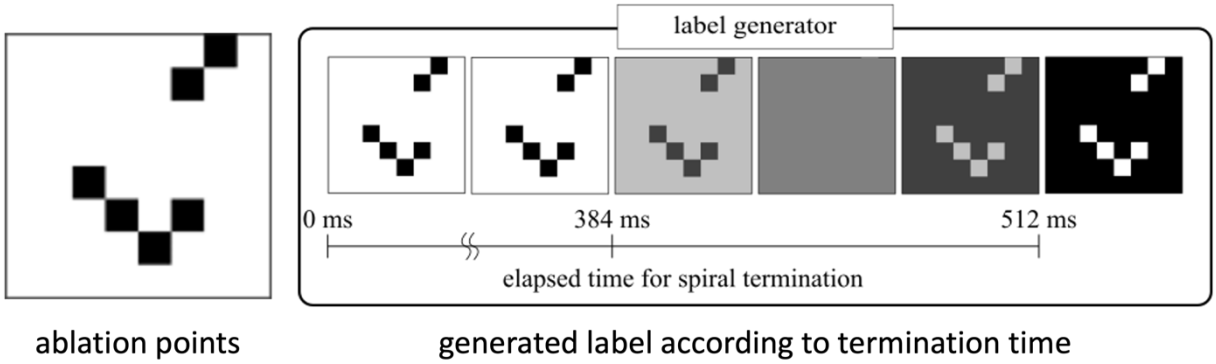

Figure 2.5 Labels based on simulation result of proposed ablation

2.2.3 Learning conditions

By comparing the above labels with the output of the DAM, it may be possible to learn the ablation sites to stop the spiral excitation, but on the other hand, if the optimization is conducted to minimize only this comparison, the strategy to ablate the entire area will be a different optimal solution. However, in the treatment of cardiac ablation, a small ablated area is preferable because it is known that an excessively large ablated area can lead to a decrease in cardiac function. Therefore, the loss function was designed not only to stop the spiral excitations but also to keep the ablated area small.

The mean absolute error (MAE) between the model output and the corresponding label and the L1 norm of the model output were used as the loss function for training (Equation 2.4). The MAE was used to measure the difference between the model output and label, i.e., for repeating a successful ablation pattern. The L1 norm was set to reduce the sum of the DAM output and to keep the ablated area small.

$$L = \frac{1}{64}\sum_{i,j=0,0}^{7}\left|A(i,j) - \hat{A}(i,j)\right| + \frac{\lambda}{64}\sum_{i,j=0,0}^{7}\left|\hat{A}(i,j)\right| \tag{3}$$

Here, L is the loss, $\hat{A}(i,j)$ is the output of the DAM at point (i,j), $A(i,j)$ is the label value at point (i,j), and λ is the regularization parameter, which determines the ratio of the two types of loss functions. In this study, regularization parameter was set to 0.25, 0.4, 0.5, and 1.0. Adam

optimizer with a learning rate of 0.001 was used as an optimization function. Batch size was set to 5, and the number of epochs was set to 2000. To speed up the learning process, the five simulations in the mini-batch were run in parallel. All experiments were performed in Python using Pytorch [70] on a Linux Server (Ubuntu 18.04.3 LTS) with 5 GPUs (NVIDIA GeForce RTX 2080).

2.2.4 Evaluation method

To evaluate the DAMs obtained by training, evaluation experiments were conducted using 340 test data cases. As the trained DAM, the model with the smallest loss to the validation data was basically used. However, if the model with the smallest loss chose not to ablate anywhere, to evaluate the performance of the ablation proposed by the model, DAMs in previous epochs were checked. Among the models which chose to perform ablation, the one at the closest epoch to the epoch of the model with the smallest loss was used as the trained DAM.

Two other ablation strategies were used for comparison with the trained DAM: random ablation (RND) and rotor ablation (ROT). In RND, a random value array comprising 8 pixels × 8 pixels was first generated, and the random ablation pattern was determined. This was performed by selecting the same number of points as the trained DAM ablation from the pixels with the highest value. ROT is an ablation strategy to target the center of spiral excitation and is often used in clinical practice [71]. In this study, the position of the spiral center was quantitatively detected using an analysis called phase variance [72]. The ablation area was then determined by thresholding the time average of the phase variance of the spiral excitation before ablation, which has the characteristic of being higher in the spiral center. The value of the time average of the phase variance ranges from 0 to 1. The threshold value used to detect the spiral center was experimentally set to 0.5 in this study to be equivalent to the ablation size of the trained DAM.

For these three ablation strategies, the excitation after ablation for 1000 ms on 340 cases of test data were simulated. As in training, the termination of the spiral excitation was judged by whether the maximum value of the membrane potential in the simulation area was below -40 mV, the ratios of spiral termination of the three different ablation strategies were compared.

2.3 Results

2.3.1 Model transition during learning process

Figure 2.6, 2.7, and 2.8 show the results for the transition of the ablation strategy when training with the regularization parameter $\lambda = 0.5$. First, Figure 2.6 shows the ablation by the DAM at the end of 10 epochs for the three cases in the validation data. The number in the lower right corner of each image indicates the time that has elapsed since the ablation was performed. As can be seen from the figure, the model at the beginning of learning ablated almost the entire region, regardless of the excitation mode, and stopped the spiral excitation.

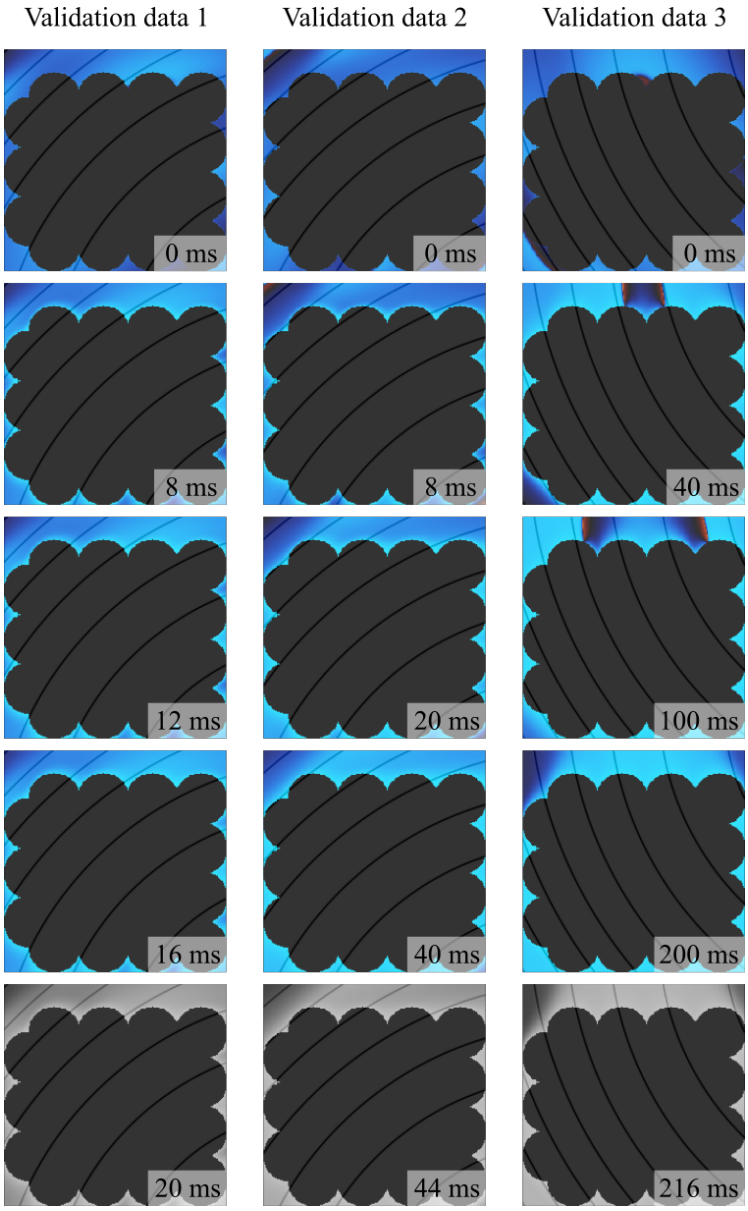

Figure 2.6 Ablation example for validation data (after 10 epochs)

Figure 2.7 shows the ablation proposed by DAM after 1000 epochs for the same validation data as Figure 2.6. From this result, it was found that the DAM chose not to ablate for the validation data 2, and that the other two cases were ablated in a single vertical line to stop the spiral excitation.

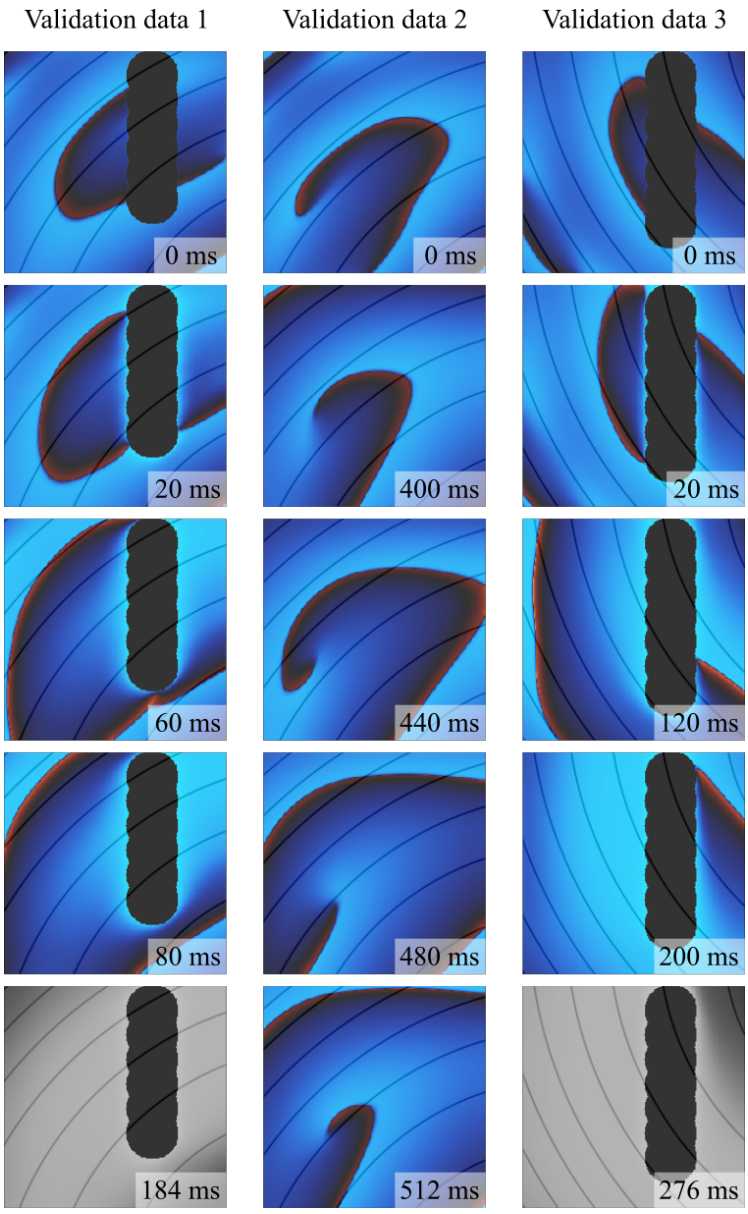

Figure 2.7 Ablation example for validation data (after 1000 epochs)

Finally, here is the ablation results by a model after 2000 epochs learning. It was found that the trained DAM stopped the spiral excitations with only one or two points of ablation. These figures indicate that the DAM may be able to stop the spiral excitation with fewer cauterization points with learning process.

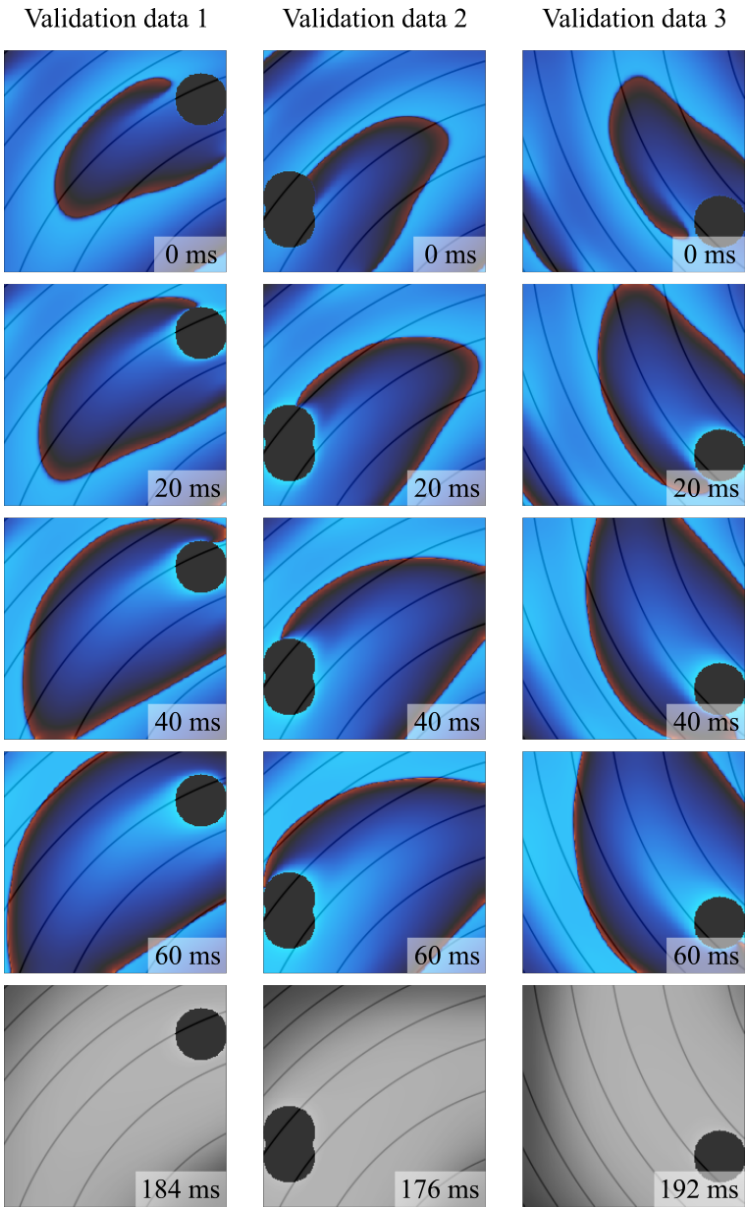

Figure 2.8 Ablation example for validation data (after 2000 epochs)

2.3.2 Comparison of ablation strategies

Figure 2.7 and Figure 2.8 shows two examples of the ablation results using three different ablation strategies. In these figures, time-series images of membrane potentials during spiral excitation without ablation, and after ablation by RND, ROT, DAM are shown, and fiber orientation and ablated area (black circles) is overlayed. The time shown in the lower left corner of each image indicates the time elapsed since the ablation was performed. For example, from top panel of Figure 2.7, there was one clockwise spiral excitation near the center of the simulated region. The result showed that RND was unable to affect the original spiral excitation, and a phenomenon called anatomical reentry, in which spiral excitation moves around the ablated area, occurred in ROT, while only DAM swept the spiral excitation toward the boundary of simulated area and stopped it. Figure 2.8 shows an example of relatively complex excitation with two spiral excitations, but as in Figure 2.7, only ablation proposed by DAM could stop the spiral excitations. These two typical cases indicate that DAM ablation may be superior to the two ablation strategies compared in terms of spiral termination.

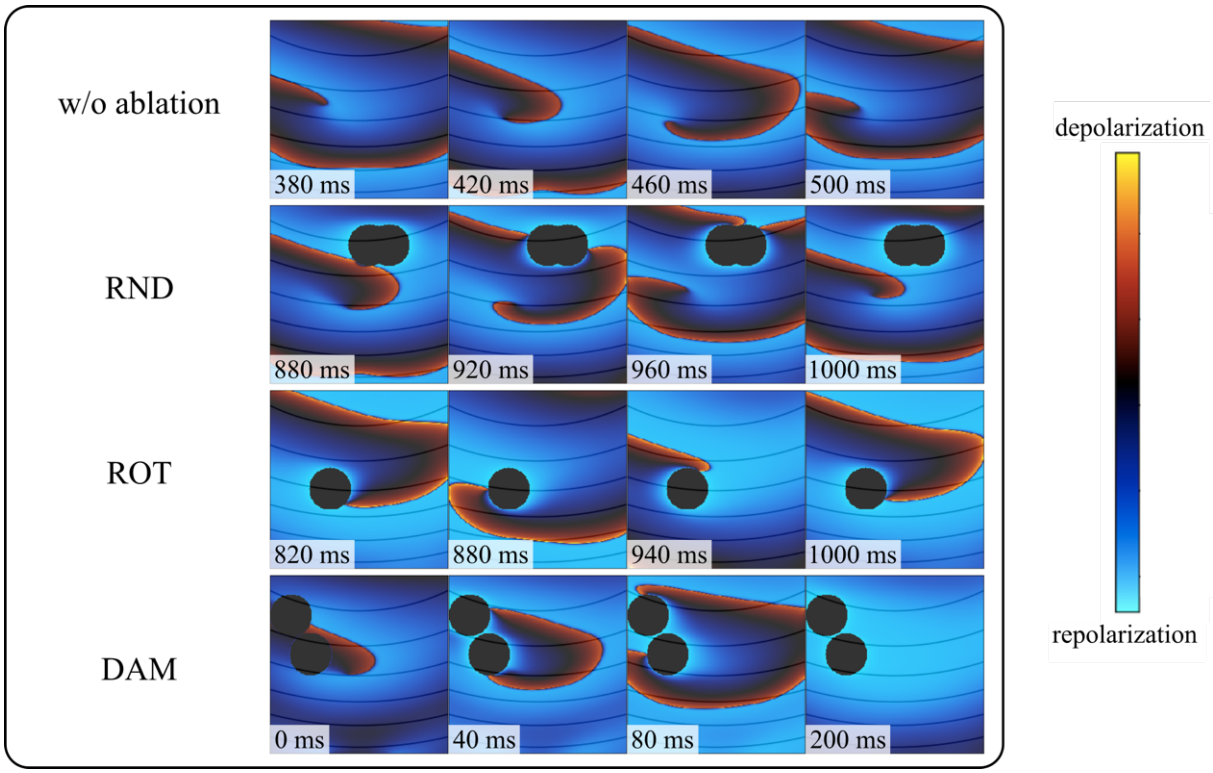

Figure 2.9 Comparison of the three ablation strategies (single spiral excitation)

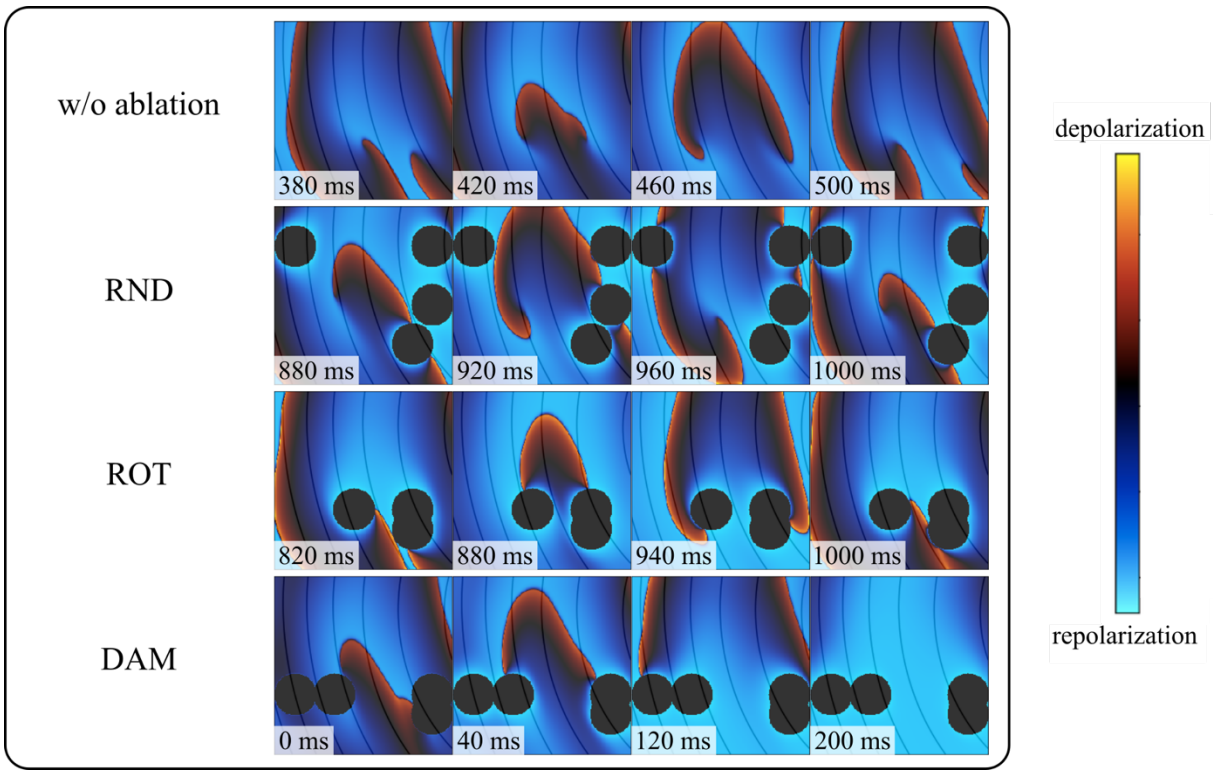

Figure 2.10 Comparison of the three ablation strategies (double spiral excitations)

Next, an analysis was performed to quantitatively evaluate the effects of the three ablation strategies. In order to compare the effects of ablation quantitatively, the changes in cardiac excitation caused by ablation were classified into three categories: ‘no effect’, ‘anatomical reentry’, and ‘termination’. Figure 2.9 shows typical isochronal maps and the time series of the membrane potential for the three phenomena. As shown in this example, the case in which the spiral reentry remained in the same place even after ablation was classified as 'no effect', and the case in which the spiral excitation circles around the ablated area was classified as 'anatomical reentry'. In the case of ‘Termination’, the spiral excitation was swept to the boundary of the simulated area.

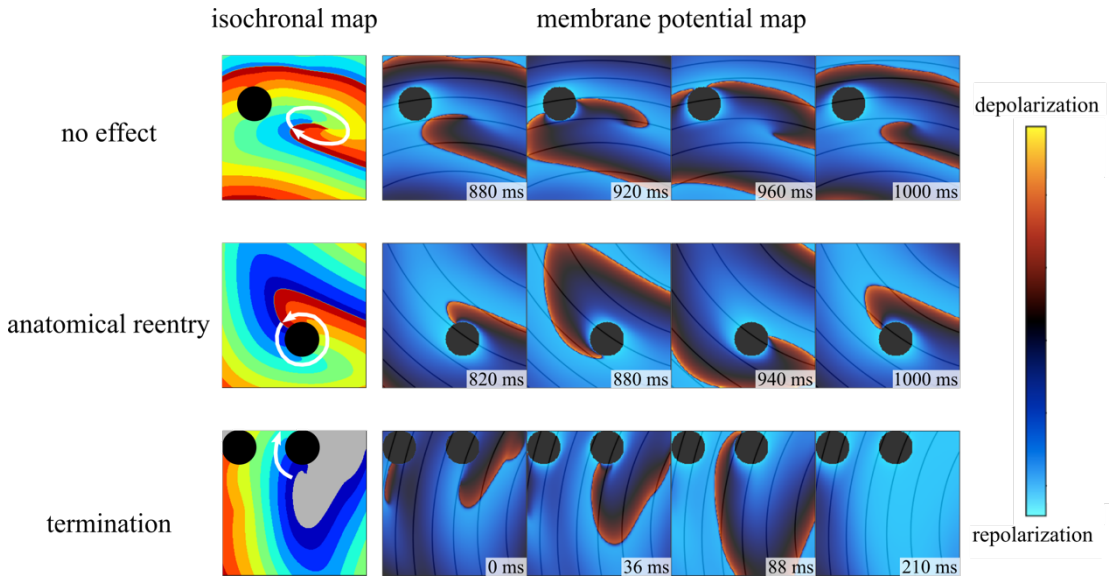

Figure 2.11 Classification of ablation effect

Based on the classification mentioned above, a quantitative comparison of the effects of the three ablation strategies on the 340 test data cases is shown in Figure 2.10. In the analysis, DAM trained with $\lambda = 0.5$ was used as trained DAM. Accordingly, in RND, the most common category was 'no effect,' with a percentage of 64.4%. In ROT, 'anatomical reentry' was observed in 90.6% of cases, and in DAM, 'termination' was observed in 75.6%. In RND and ROT, spiral excitation was terminated in 12.6% and 8.5% of cases, respectively.

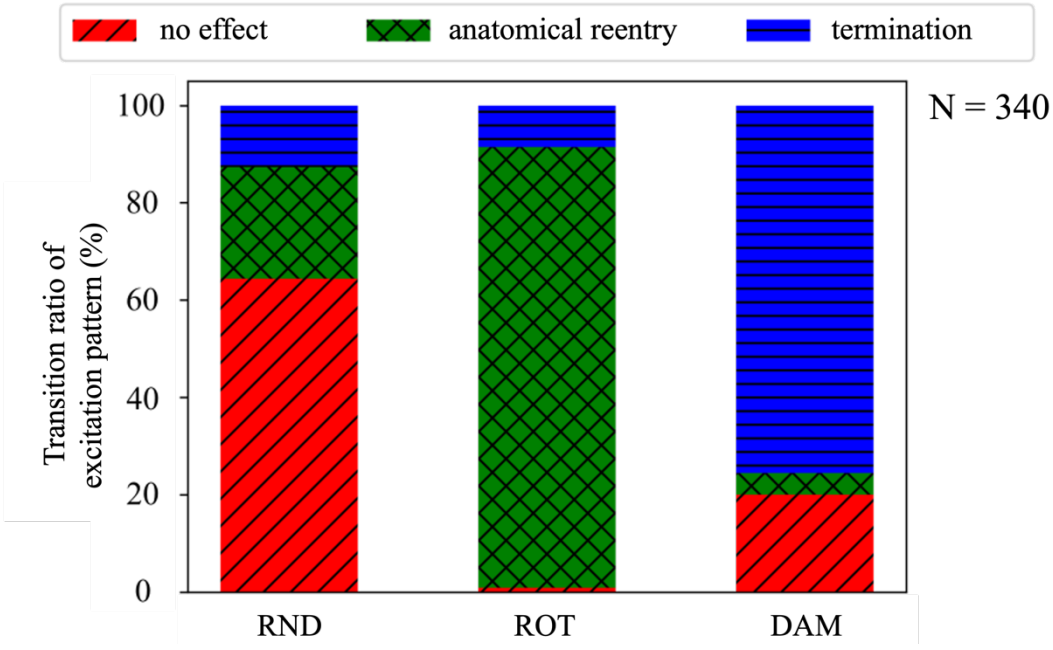

Figure 2.12 Effect of each ablation strategy

On the other hand, the ablation area of RND, ROT, and the DAM were calculated as 7.0 ± 2.8%, 12.5 ± 5.7%, and 6.5 ± 2.4%, respectively (Figure. 2.11). From these results, it was clear that the ablation by DAM achieved a higher termination rate of spiral excitations in a comparable ablation area size compared to the other two ablation strategies.

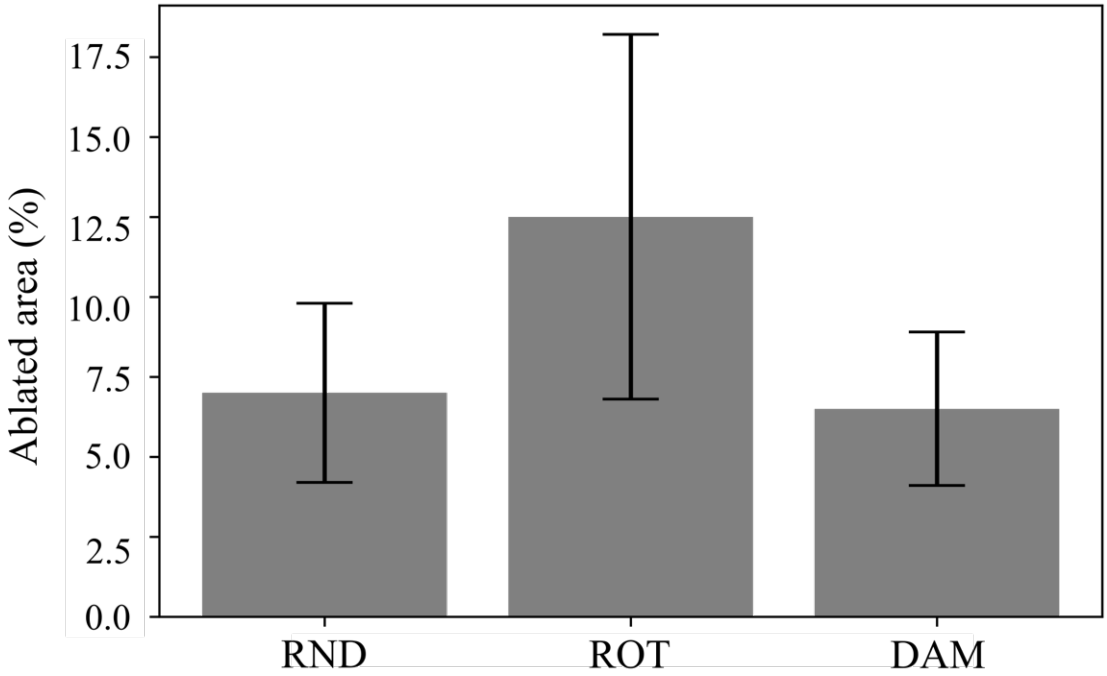

Figure 2.13 Ablation area percentages of three ablation strategies

Next, the spatial bias of the ablated area by the three ablation strategies is visualized in Figure 2.12. From the result, it appeared that RND showed uniform ablation over the entire region, while ROT showed frequent ablation in the center of the simulation region except for the boundary, and conversely, ablation tended to be performed near the boundary in DAM. In order to quantitatively evaluate the bias of the ablated area, the (8 pixels × 8 pixels) candidate ablation points were divided into four regions as shown in the left figure of Figure 2.13, and the percentage of ablating each region was calculated. This result quantitatively showed that RND ablated the four areas almost equally, while ROT had a small percentage of region 1, which is near the boundary of the simulation area, and the DAM had a large percentage of region 1.

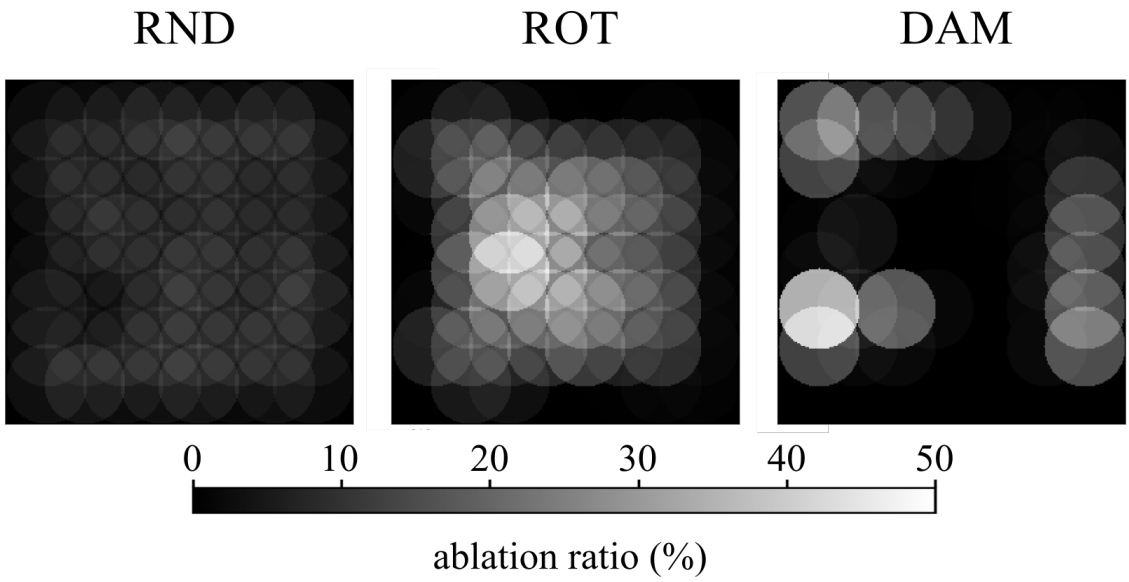

Figure 2.15 Spatial bias of the ablated points by three ablation strategies

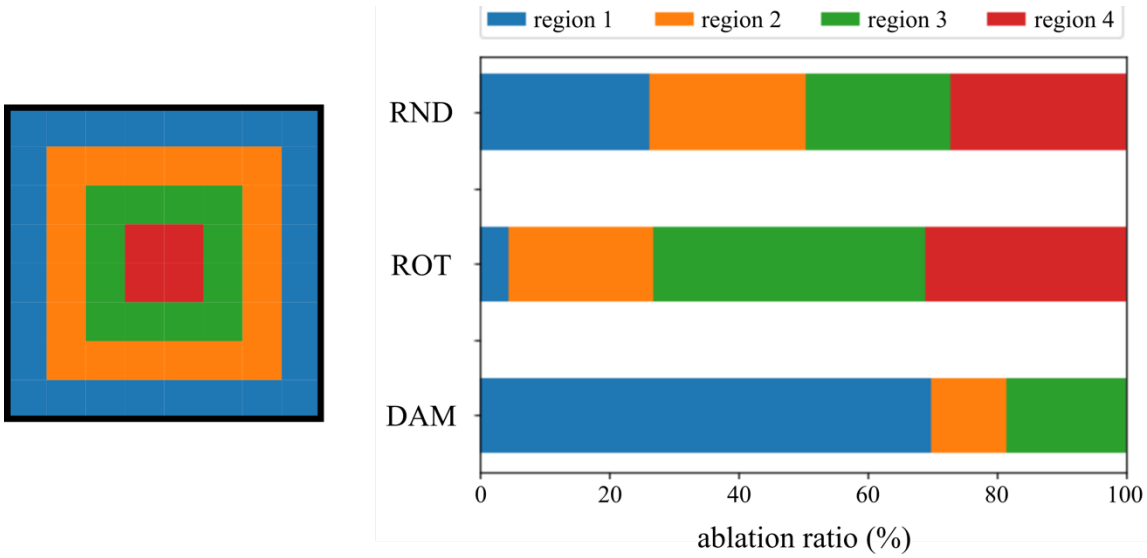

Figure 2.14 Quantitative evaluation of spatial bias of ablated area

Figure 2.14 shows a histogram of the minimum distance between the trajectory of the spiral center and the center of each ablation point. In the ROT, which aims to ablate near the spiral center, the position of the ablation points and the center of rotation were very close. However, in the trained DAM, the distribution had a peak at approximately 5 mm, and in the RND, the distribution appeared relatively even with no apparent peak.

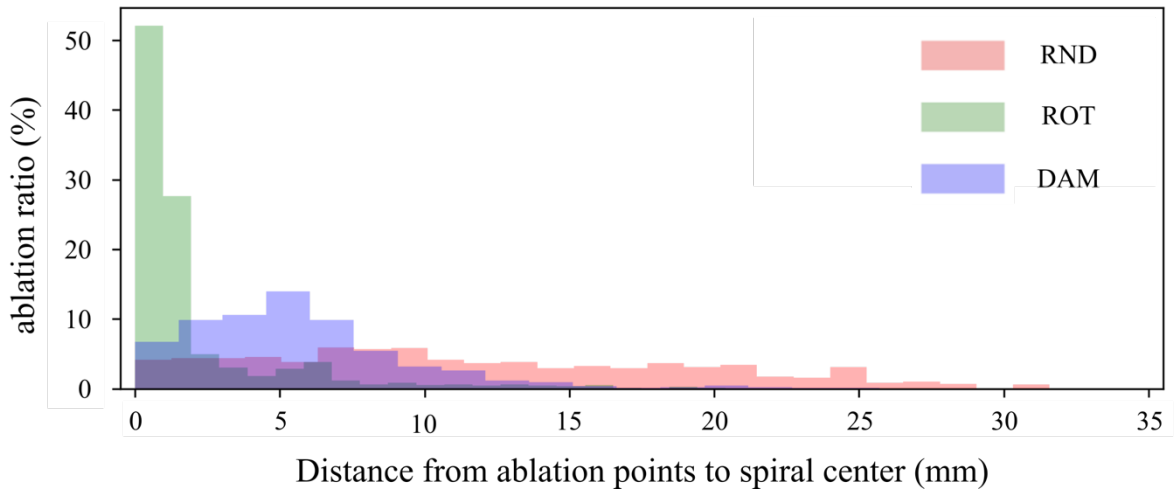

Figure 2.16 Comparison of distance from ablation points to spiral center

2.3.3 Difference in learning result by regularization parameter

Figure 2.15 shows an example of ablations by DAMs trained with various regularization parameters. From this figure, it was apparent that the model trained with λ set to 0.25 ablated almost the entire region and terminated the spiral excitation at approximately 128 ms after the ablation. In the model with λ set to 1.0, the left side of region was ablated, but the original spiral excitation was sustained. On the other hand, although the trained model with λ set to 0.5 ablated only two points, the proposed ablation successfully terminated the spiral excitation at around 400 ms after ablation.

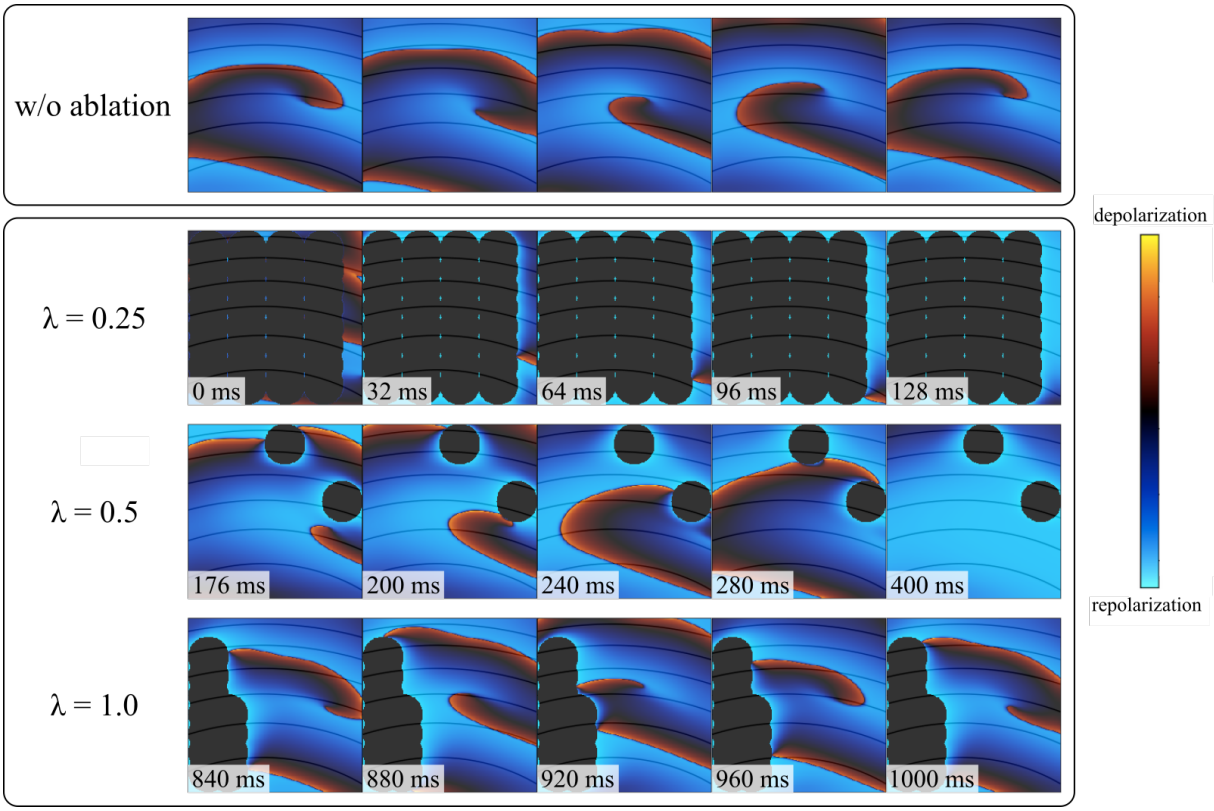

Figure 2.17 Example of ablation proposed by DAMs trained with different regularization parameters

Moreover, from Figure 2.16, it was found that the regularization parameter appeared to influence the learning results, and the spiral termination rate tended to increase when the ablation area was increased. The ablation ratio of each regularization parameter (0.25, 0.4, 0.5, and 1.0) was 84.1%, 16.2%, 6.5%, and 21.4%, respectively, and termination rate was 99.1%, 59.7%, 74.1%, and 37.4%, respectively.

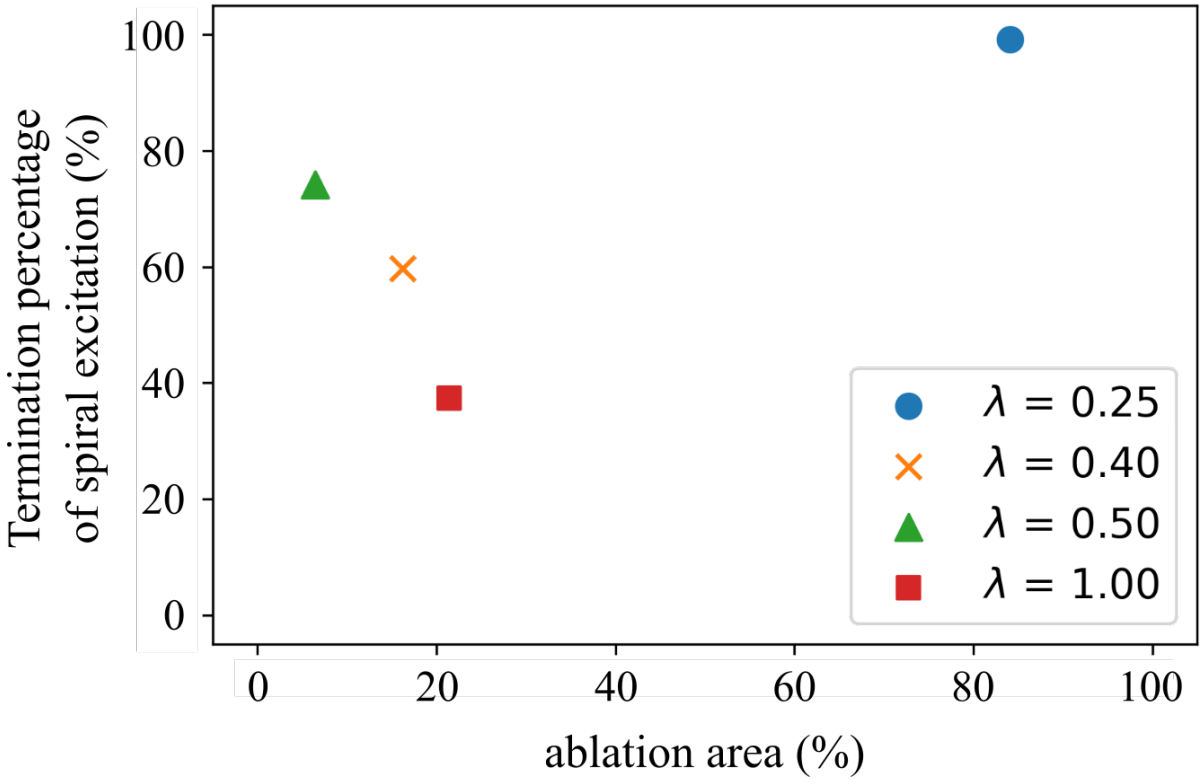

Figure 2.18 Termination percentage and ablation area of DAMs trained with different regularization parameters

2.4 Discussion

2.4.1 The possibility of optimizing the ablation strategy

In this chapter, an *in silico* reinforcement learning scheme for optimizing the ablation sites has been constructed and experiments have been conducted for proof of concept. First, when comparing the trained DAM with the RND and the ROT, it was found that the trained DAM achieved ablation area percentage of 6.5 ± 2.4% and spiral termination percentage of 75.6%, and the termination percentage was superior to the other two ablation strategies (RND: 12.6%, ROT: 8.5%) as shown in Figure 2.10 and Figure 2.11. By comparing the ablation patterns of each ablation strategy, it can be seen that the trained DAM tended to ablate the area around the tissue boundary (Figure 2.12 and Figure 2.13). Moreover, although not as much as the ROT, compared to RND, the trained DAM tended to ablate the area near the center of the spiral excitation (Figure 2.14). Comparing the learning results with different regularization parameters λ, it was clear that the performed ablation and the respective effects varied greatly depending on the parameter (Figure 2.15 and Figure 2.16). These results suggested that, although some adjustment of the regularization parameter is essential for proper learning, it is thought that the trained DAM adaptively determined the appropriate ablation points for terminating the spiral excitation according to the excitation pattern. Therefore, it can be said that *in silico* learning showed the possibility of optimizing the ablation sites through trial and error without relying on prior knowledge.

2.4.2 Interpretation of obtained ablation strategy

By comparing three ablation strategies, it was clear that ablations proposed by the trained DAM tended to be located near the spiral center and around the tissue boundary (Figure 2.12, Figure 2.13, and Figure 2.14). Here, the electrophysiological interpretation of ablation strategies obtained by *in silico* learning will be discussed.

There have been many previous study to effectively move and stop the spiral excitations, especially for low-energy defibrillation using electrical current stimulation, and the mechanism of the movement has previously been discussed [66], [73]. In these studies, they found that it is necessary to generate new spiral excitations and interfere with the original spiral wave to effectively shift the spiral wave. On the other hand, it is widely accepted that a discontinuity in the wavefront causes a phenomenon called wavebreak, which leads to new spiral excitations [74] and the wavebreak was also observed around the ablated area in our simulation. Therefore, ablating near the spiral excitation is expected to generate wavebreak-derived spiral excitations, and these are expected to shift the original spiral excitation through interference. Figure 2.17 shows a schematic diagram of cardiac excitation when ablation is performed near the spiral center. As shown in Figure 2.17a, the case where there is a clockwise spiral excitation and ablation is conducted near the spiral center is considered. It is thought that wave break generates two spiral excitations when the excitation wavefront enters the ablated area (Figure 2.17b), and

one of them annihilates the original spiral excitation (Figure 2.17c), causing the clockwise spiral excitation to appear to move into the ablated region (Figure 2.17d).

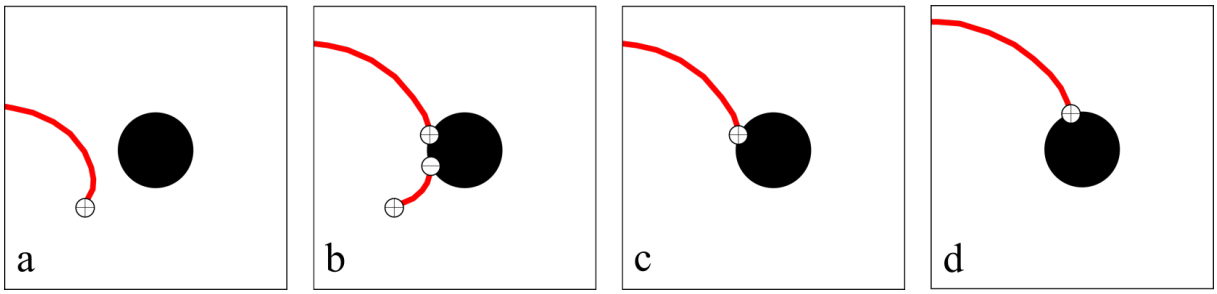

Figure 2.19 Schematic diagram of changes in cardiac excitation
after ablation near the spiral center

On the other hand, a schematic diagram of clockwise spiral excitation when ablation is far from the original spiral excitation is shown in Figure 2.18. In this case, as in the case of ablation near the spiral center, the wave break occurs and generates two spiral excitations (Figure 2.18b). However, if the original spiral excitation is not sufficiently close to the ablated area, the newly generated spiral excitations may annihilate each other (Figure 2.18c), and the original spiral excitation may itself persist (Figure 2.18d). The above discussion suggests that ablation near the spiral center is essential for shifting the spiral excitation.

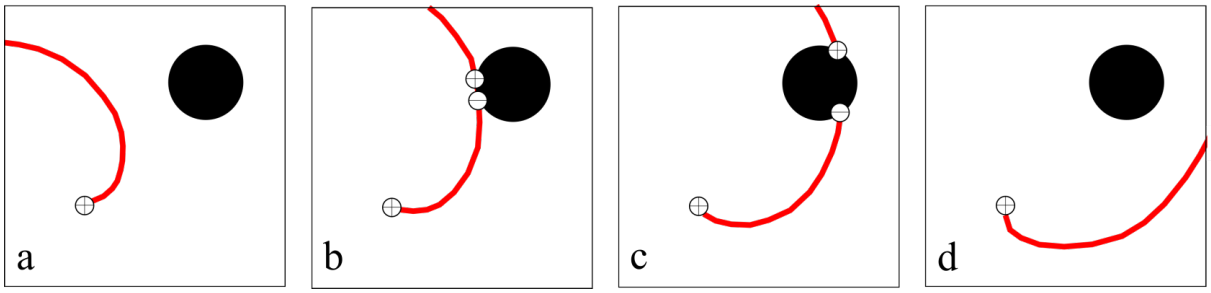

Figure 2.20 Schematic diagram of changes in cardiac excitation
after ablation far from the spiral center

Nevertheless, ablation near the spiral center does not necessarily terminate the spiral excitation. In fact, termination rate of the ROT, which targets the spiral center, was 8.5%, and 90.5% of the test data resulted in anatomical reentry after the ROT, as seen in Figure 2.7 and Figure 2.8. This failure can be solved by connecting the ablation region to the tissue boundary, because in anatomical reentry, spiral excitation moves around the ablated region. Hence, if the tissue boundary is in the middle of the path, the spiral excitation cannot be sustained. These considerations suggest that it is also important to connect the ablation area to the tissue boundary

to terminate the spiral excitation, and it is likely that the DAM had acquired the knowledge of connecting the ablated area to the boundary from the *in silico* reinforcement learning.

The ablation strategy obtained in this study may be similar to those proposed in previous studies. In fact, the ablation strategy obtained in this study can be classified as linear ablation, and it has also already been proposed to connect linear ablation to the tissue boundary, as described in Introduction. On the other hand, it is of high interest that the reinforcement learning method, which is not bound by prior knowledge, selected a similar ablation strategy from a huge number of ablation pattern candidates. In addition, while conventional linear ablation mainly focuses on anatomical features to determine the ablation site, the findings of this study suggest that the ablation should be performed near the spiral center. Therefore, it can be said that the excitability of the heart, including the location of the spiral excitation, should be considered to improve the therapeutic effect of tachyarrhythmia.

2.4.3 Failed cases of spiral termination

As shown in Figure 2.10, the learned DAM with $\lambda = 0.5$ achieved spiral termination rate of 75.6% (257/340), meaning that the trained DAM failed to terminate spiral excitations in 24.4% of the test data (83/340). Figure 2.19 shows the results of classifying the failed examples. There were cases where the ablation area was far from the rotation center and did not affect the spiral excitation (Fig. 2.19A), cases where the ablation was near the rotation center but not connected to the boundary (Fig. 2.19B), and cases where the ablation could not terminate one of the two spiral excitations (Fig. 2.19C). The ratio of each unsuccessful case was 34.9% (29/83), 22.9% (19/83), and 42.2% (35/83), respectively. Therefore, in approximately half of the failed cases (48/83), ablation from near the spiral center to the tissue boundary was not achieved. The reason for this failure could be the small number of training datasets and insufficient tuning of the hyperparameters. In this study, the number of spiral excitations used for training was limited to 120 cases to reduce the learning cost, but this number of training data may have been insufficient to acquire sufficient generalization performance. In addition, only four regularization parameters were considered in this study, but there is a possibility that even better DAM can be acquired by tuning these hyperparameters as well. The other half of the failed cases (35/83) had complex excitation patterns with multiple spiral excitations present. This may be due to the complexity of the data used for training. In fact, out of the 120 spiral excitations in the training data, there were 27 cases with multiple spirals, and the rest were relatively simple excitation patterns with a single spiral excitation. Therefore, to improve the termination percentage for more complex excitations, it is necessary to increase the number of complex excitations in the training data.

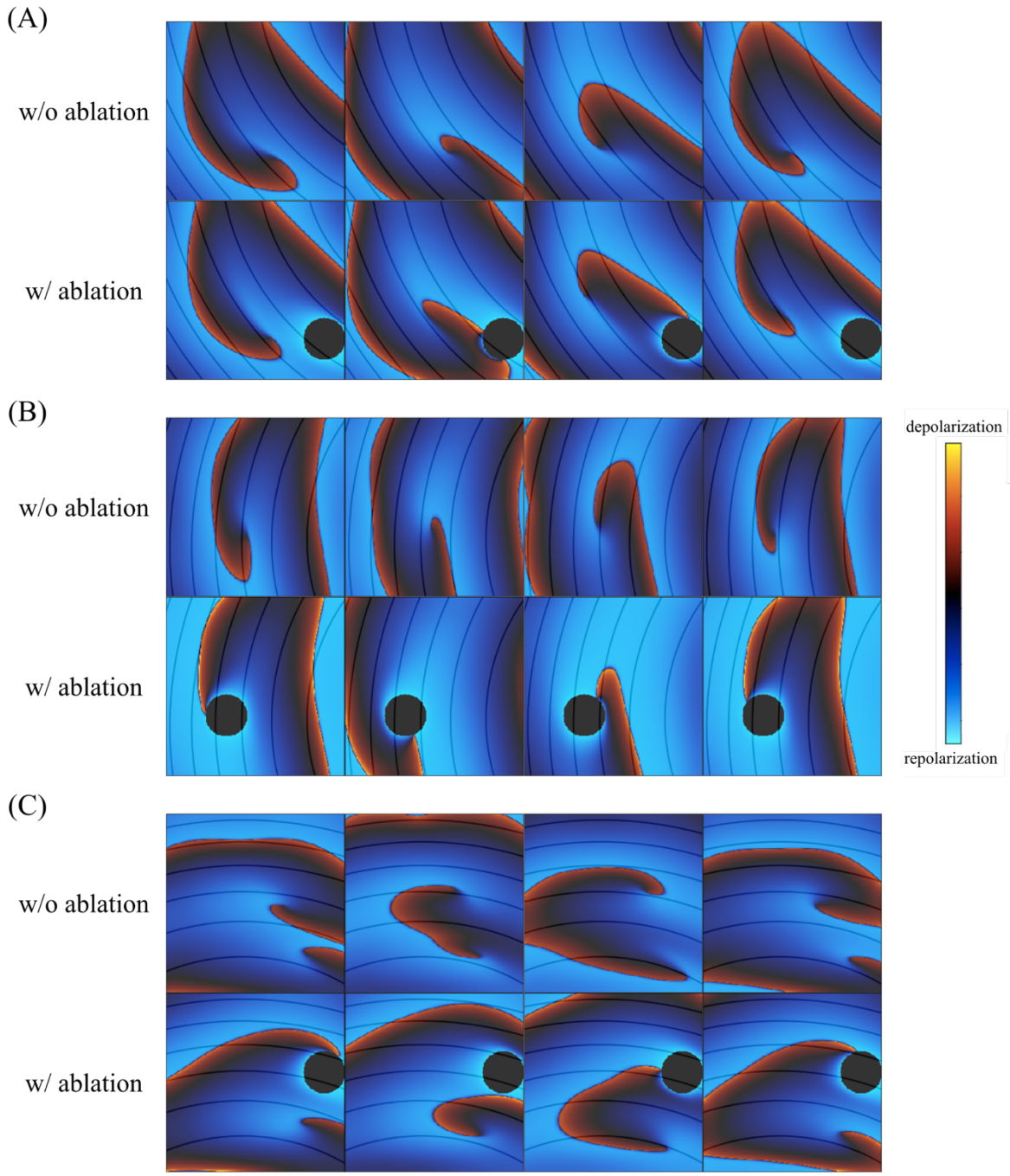

Figure 2.21 Example of a trained DAM failing to stop spiral excitation

2.4.4 The effect of regularization parameter

As shown in Figure 2.15 and Figure 2.16, the learning results highly depended on the value of the regularization parameter. These results can be explained by considering the effect of the regularization parameter on the loss. As shown in Equation 2.4, regularization parameter λ is the parameter that determines the balance between the MAE and the L1 norm.

For example, when the regularization parameter is small, the MAE had a relatively larger impact on the loss compared to the L1 norm. In this instance, terminating the spiral excitation became a higher priority than keeping the ablation area small. According to Figure 2.16, when the model was trained with $\lambda = 0.25$, the spiral termination rate was 99.1% while the ablation area percentage was also 84.1%. This indicated that the objective of keeping the ablation area small was not achieved.

On the other hand, when the regularization parameter is large, the DAM would prioritize L1 norm reduction over MAE reduction, resulting in convergence to a strategy of no ablation at all. In fact, Figure 2.20, which indicates the transition of the termination rate of spiral excitation and the ablation percentage during learning process, shows that these two values converge to 0%, that means the converges to no ablation. In Figure 2.16, the ablation rate of the DAM trained with $\lambda = 1.0$ was about 20%, but this may be due to the fact that the DAM that always performed ablation was selected as a trained model. As a result of adopting the output of a DAM which did not learn sufficiently, the ablation area percentage was approximately 20% and the spiral termination rate was approximately 40%.

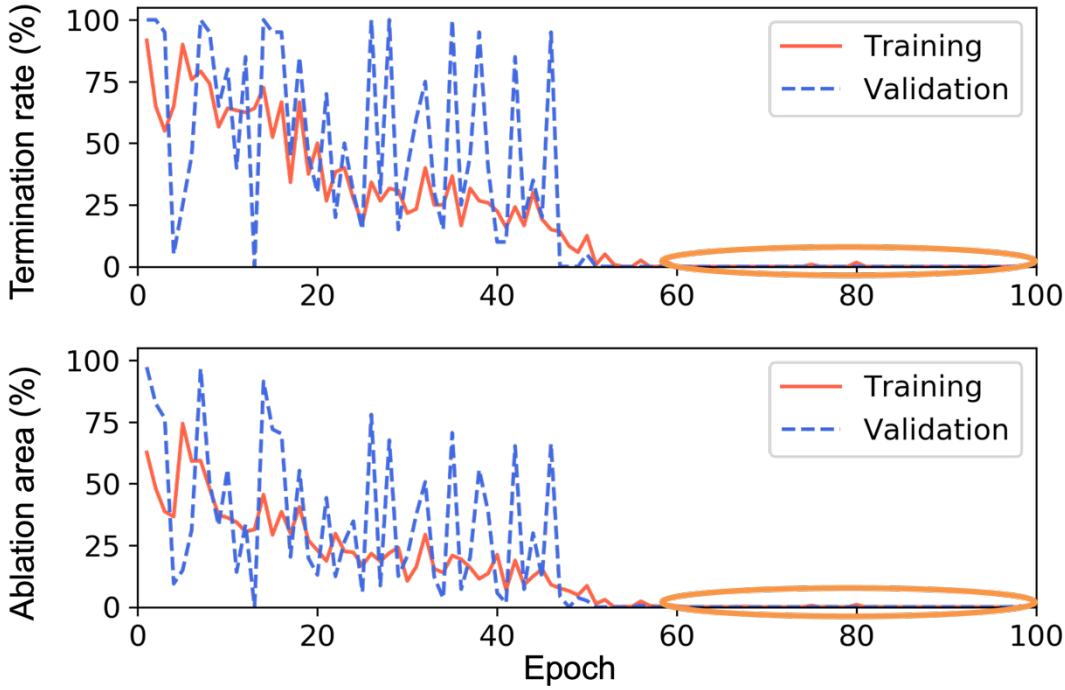

Figure 2.22 transition of the termination rate and ablation percentage ($\lambda = 1.0$)

When $\lambda = 0.4$, as in the case of $\lambda = 0.5$, the learning was continued without getting interrupted by the local solution. Both the ablation area percentage and spiral termination rate were not as positive as the learning results of $\lambda = 0.5$. Considering the above points, some adjustment of the regularization parameter is necessary for proper learning, and effective hyperparameter tuning for the regularization parameter needs to be considered.

2.4.5 Limitations

The optimization of the ablation sites were attempted by *in silico* learning, but there are still limitations to apply the *in silico* learning scheme to actual clinical practice.

The first limitation is the complexity of the electrophysiology simulator used in this study. In order to demonstrate the proof of concept of the proposed method, a simple 2D cardiac simulator was used to reduce the calculation time for each simulation. However, it is clear that cardiac excitation is more complex due to anatomical and electrophysiological heterogeneity, which is caused factors such as the variation in myocardial thicknesses [75], the presence of curvatures [76], and fibroblast expression [77]. Therefore, 2D tissue with uniform myocardial properties used in this study can reproduce relatively simple spiral excitations, but cannot adequately simulate the complex excitation phenomena such as ectopic activity and multiple wavelet reentry, which are known to occur in cardiac tissue [78].

The second limitation is the degree of freedom of ablation. In this study, in order to control the search space for optimization, the sequence of ablation points was not optimized, and the all ablations are performed simultaneously. Simultaneous ablation is equivalent to optimizing the modification of excitable media to prevent sustained spiral reentry excitation, which is important in terms of controlling the myocardial tissue to prevent recurrence of the spiral excitation. On the other hand, in the clinical ablation procedure, it is difficult to ablate multiple points at the same time, and it is necessary to ablate each point in turn. When performing ablation at each location, the excitatory state may change with each ablation, and depending on the order of ablation, the excitatory state may become unexpectedly complicated. For this reason, the sequence of ablation points should also be optimized for clinical application. Furthermore, in this study, ablation was modeled as a complete death of cardiomyocytes, but in actual ablation procedures, the degree of ablation may also be a variable and may be subject to optimization. By including the degree of ablation in the optimization target, it may be possible to establish a better ablation strategy. However, in order to optimize the degree of ablation by *in silico* learning, it is necessary to reproduce the continuous degeneration of cardiomyocytes during ablation on a simulation model. The electrophysiological changes of cardiomyocytes during the process of ablation have not been well studied so far, so it is necessary to model the behavior of cardiomyocytes during ablation and incorporate the cell model into the cardiac simulator for optimizing the degree of ablation.

2.5 Summary

In this chapter, an *in silico* reinforcement learning was applied for optimization of ablation strategy, and as a proof of concept, *in silico* learning using 2D cardiac simulator was conducted.

The deep neural network-based ablation model (DAM) was designed to input a membrane potential movie and output an ablation preferability. As a virtual environment for *in silico* learning, a 2D monodomain cardiac tissue model, which has relatively low computational cost than bidomain model was constructed and used. In order to learn ablation sites that effectively stop spiral excitation with small ablated area, the sum of the mean absolute error between the DAM output and the label and L1 norm of the DAM output was used as the loss function, and the DAM was trained. After training, the trained DAM was compared with two different strategies: the random ablation strategy (RND) and the rotor ablation strategy (ROT).

The results showed that the percentages of ablation areas of RND, ROT, and best trained DAM were 7.0±2.8%, 12.5±5.7%, and 6.5±2.4%, respectively, and the termination rates of spiral excitation were 12.6%, 8.5%, and 74.1%, respectively. After evaluating the ablation strategy obtained by learning, the DAM learned to effectively terminate spiral excitations by ablating the area from near the spiral center towards the tissue boundary without any prior knowledge. Although the obtained ablation strategy as the *in silico* learning was similar to the linear ablation already proposed, it is of high interest that the reinforcement learning method, which is not bound by prior knowledge, selected a similar ablation strategy from a huge number of ablation pattern candidates. Furthermore, although conventional linear ablations were based on anatomical information, this study showed that linear ablation that takes into account the excitability of the heart, including the location of the spiral excitation may be effective.

Although some limitations remain, such as the complexity of the cardiac simulator and the degree of freedom of the ablation, this chapter showed the possibility that in silico learning can be used to optimize the ablation pattern for effective termination of the tachyarrhythmia.

Chapter 3 System construction for *in vitro* experiment

This item was excluded because it is expected to be published in the future.

Chapter 4 Validation experiment using human iPSC heart tissue

This item was excluded because it is expected to be published in the future.

Chapter 5 General discussion

5.1 Potential for *in silico* optimization of ablation strategy

This item was excluded because it is expected to be published in the future.

5.2 Limitations

The optimization of the ablation sites were attempted by *in silico* learning, but there are still limitations to apply the *in silico* learning scheme to actual clinical practice.

5.2.1 Complexity of the cardiac simulator

In order to demonstrate the proof of concept of the proposed method, a simple 2D cardiac simulator was used to reduce the calculation time for each simulation. However, it is clear that cardiac excitation is more complex due to anatomical and electrophysiological heterogeneity, which is caused factors such as the variation in myocardial thicknesses [Augustin 2020], the presence of curvatures [Song 2018], and fibroblast expression [Tanaka 2007]. Therefore, 2D tissue with uniform myocardial properties used in this study can reproduce relatively simple spiral excitations, but cannot adequately simulate the complex excitation phenomena such as ectopic activity and multiple wavelet reentry, which are known to occur in cardiac tissue [Nattel 2008].

On the other hand, in recent years, the use of personalized models, which include not only the structure of cardiac tissue but also the distribution of fibroblasts, has become the mainstream methodology of in-silico research [Aronis 2019]. By using such a complex and life-like cardiac simulator that takes into account structural and electrophysiological heterogeneities, it is possible to obtain membrane potential information of complex cardiac excitations with high spatiotemporal resolution. The problem of using a personalized model is that it is expected to increase the computational cost. However, there have been many studies on speeding up computer simulations in recent years [], and it is not impossible to perform *in silico* learning using a complex and life-like cardiac simulator by applying such techniques.

5.2.2 Degree of freedom of ablation

In this study, in order to control the search space for ablation site optimization, the sequence of ablation points was not optimized, and the all ablations are performed simultaneously. Simultaneous ablation is equivalent to optimizing the modification of excitable media to prevent sustained spiral reentry excitation, which is important in terms of controlling the myocardial tissue to prevent recurrence of the spiral excitation. On the other hand, in the clinical ablation procedure, it is difficult to ablate multiple points at the same time, and it is necessary to ablate each point in turn. When performing ablation at each location, the excitatory state may change with each ablation, and depending on the order of ablation, the excitatory state may become unexpectedly complicated. For this reason, the sequence of ablation points should also be optimized to make the proposed method applicable to clinical practice.

Furthermore, in this study, ablation was modeled as a complete death of cardiomyocytes, but in actual ablation procedures, the degree of ablation may also be a variable and may be subject to optimization. However, in order to optimize the degree of ablation by *in silico* learning, it is necessary to reproduce the continuous degeneration of cardiomyocytes during ablation on

a simulation model. The electrophysiological changes of cardiomyocytes during the process of ablation have not been well studied so far, so it is necessary to model the behavior of cardiomyocytes during ablation and incorporate the cell model into the cardiac simulator for optimizing the degree of ablation.

5.2.3 Improvement of ablation system

This item was excluded because it is expected to be published in the future.

Chapter 6 Conclusion

This item was excluded because it is expected to be published in the future.

Bibliography

[1] A. S. Amin, H. L. Tan, and A. A. M. Wilde, “Cardiac ion channels in health and disease,” *Hear. Rhythm*, vol. 7, no. 1, pp. 117–126, Jan. 2010.

[2] A. S. Adabag, R. V. Luepker, V. L. Roger, and B. J. Gersh, “Sudden cardiac death: epidemiology and risk factors,” *Nat. Rev. Cardiol. 2010 74*, vol. 7, no. 4, pp. 216–225, Feb. 2010.

[3] J. Andrade, P. Khairy, D. Dobrev, and S. Nattel, “The clinical profile and pathophysiology of atrial fibrillation: relationships among clinical features, epidemiology, and mechanisms.,” *Circ. Res.*, vol. 114, no. 9, pp. 1453–68, Apr. 2014.

[4] R. G. Hart and J. L. Halperin, “Atrial Fibrillation and Stroke,” *Stroke*, vol. 32, no. 3, pp. 803–808, Mar. 2001.

[5] G. Thrall, D. Lane, D. Carroll, and G. Y. H. Lip, “Quality of Life in Patients with Atrial Fibrillation: A Systematic Review,” *American Journal of Medicine*, vol. 119, no. 5. Elsevier, pp. 448.e1-448.e19, 01-May-2006.

[6] S. Kalantarian, T. A. Stern, M. Mansour, and J. N. Ruskin, “Cognitive impairment associated with atrial fibrillation: a meta-analysis.,” *Ann. Intern. Med.*, vol. 158, no. 5 Pt 1, pp. 338–46, Mar. 2013.

[7] S. E. Wolowacz, M. Samuel, V. K. Brennan, J.-G. Jasso-Mosqueda, and I. C. Van Gelder, “The cost of illness of atrial fibrillation: a systematic review of the recent literature.”

[8] M. Zoni-Berisso, F. Lercari, T. Carazza, and S. Domenicucci, “Epidemiology of atrial fibrillation: European perspective,” *Clin. Epidemiol.*, vol. 6, no. 1, p. 213, Jun. 2014.

[9] G. Lippi, F. Sanchis-Gomar, and G. Cervellin, “Global epidemiology of atrial fibrillation: An increasing epidemic and public health challenge:,” *https://doi.org/10.1177/1747493019897870*, vol. 16, no. 2, pp. 217–221, Jan. 2020.

[10] J. E. Hall and M. E. Hall, *Guyton and Hall textbook of medical physiology e-Book*. Elsevier Health Sciences, 2020.

[11] 倉智嘉久, *心筋細胞イオンチャネル-心臓のリズムと興奮の分子メカニズム*. 文光堂, 2000.

[12] P. D. J. Gordon Betts, Kelly A. Young, James A. Wise, Eddie Johnson, Brandon Poe, Dean H. Kruse, Oksana Korol, Jody E. Johnson, Mark Womble, “Anatomy and Physiology,” *OpenStax*. [Online]. Available: https://openstax.org/books/anatomy-and-physiology/pages/1-introduction. [Accessed: 16-Nov-2021].

[13] M. of the S. Gambit, “New approaches to antiarrhythmic therapy: emerging therapeutic applications of the cell biology of cardiac arrhythmias,” *Cardiovasc. Res.*, vol. 52, no. 3, pp. 345–360, Dec. 2001.

[14] M. C. E. F. Wijffels, C. J. H. J. Kirchhof, R. Dorland, and M. A. Allessie, “Atrial Fibrillation Begets Atrial Fibrillation,” *Circulation*, vol. 92, no. 7, 1995.

[15] 井上博，村川裕二, 不整脈学. 南江堂, 2012.
[16] W. E. M. Vaughan, “Classification of antidysrhythmic drugs.,” *Pharmacol. Ther. B.*, vol. 1, no. 1, pp. 115–138, Jan. 1975.
[17] M. Lei, L. Wu, D. A. Terrar, and C. L.-H. Huang, “Modernized Classification of Cardiac Antiarrhythmic Drugs,” *Circulation*, vol. 138, no. 17, pp. 1879–1896, Oct. 2018.
[18] D. M. Roden, “Mechanisms and management of proarrhythmia,” *Am. J. Cardiol.*, vol. 82, no. 4, pp. 49I-57I, Aug. 1998.
[19] A. Al-Khadra, V. Nikolski, and I. R. Efimov, “The Role of Electroporation in Defibrillation,” *Circ. Res.*, vol. 87, no. 9, pp. 797–804, Oct. 2000.
[20] A. Cavalié, T. F. McDonald, D. Pelzer, and W. Trautwein, “Temperature-induced transitory and steady-state changes in the calcium current of guinea pig ventricular myocytes,” *Pfl{ü}gers Arch.*, vol. 405, no. 3, pp. 294–296, 1985.
[21] B. Waldecker, P. Brugada, M. Zehender, W. Stevenson, and H. J. J. Wellens, “Dysrhythmias after direct-current cardioversion,” *Am. J. Cardiol.*, vol. 57, no. 1, pp. 120–123, Jan. 1986.
[22] T. TOKANO *et al.*, “Effect of Ventricular Shock Strength on Cardiac Hemodynamics,” *J. Cardiovasc. Electrophysiol.*, vol. 9, no. 8, pp. 791–797, Aug. 1998.
[23] G. K. Larsen, J. Evans, W. E. Lambert, Y. Chen, and M. H. Raitt, “Shocks burden and increased mortality in implantable cardioverter-defibrillator patients,” *Hear. Rhythm*, vol. 8, no. 12, pp. 1881–1886, Dec. 2011.
[24] D. Scherr *et al.*, “Five-year outcome of catheter ablation of persistent atrial fibrillation using termination of atrial fibrillation as a procedural endpoint,” *Circ. Arrhythmia Electrophysiol.*, vol. 8, no. 1, pp. 18–24, Feb. 2015.
[25] J. M. Williams, R. M. Ungerleider, G. K. Lofland, and J. L. Cox, “Left atrial isolation: New technique for the treatment of supraventricular arrhythmias,” *J. Thorac. Cardiovasc. Surg.*, vol. 80, no. 3, pp. 373–380, Sep. 1980.
[26] J. L. Cox *et al.*, “The surgical treatment of atrial fibrillation: III. Development of a definitive surgical procedure,” *J. Thorac. Cardiovasc. Surg.*, vol. 101, no. 4, pp. 569–583, Apr. 1991.
[27] M. Haïssaguerre *et al.*, “Spontaneous Initiation of Atrial Fibrillation by Ectopic Beats Originating in the Pulmonary Veins,” *N. Engl. J. Med.*, vol. 339, no. 10, pp. 659–666, Sep. 1998.
[28] K. Nademanee *et al.*, “A new approach for catheter ablation of atrial fibrillation: mapping of the electrophysiologic substrate,” *J. Am. Coll. Cardiol.*, vol. 43, no. 11, pp. 2044–2053, Jun. 2004.
[29] S. M. Narayan, D. E. Krummen, K. Shivkumar, P. Clopton, W. J. Rappel, and J. M. Miller, “Treatment of atrial fibrillation by the ablation of localized sources: CONFIRM (Conventional Ablation for Atrial Fibrillation with or Without Focal Impulse and Rotor Modulation) trial,” *J. Am. Coll. Cardiol.*, vol. 60, no. 7, pp. 628–636, Aug. 2012.

[30] S. Rolf *et al.*, “Tailored atrial substrate modification based on low-voltage areas in catheter ablation of atrial fibrillation,” *Circulation: Arrhythmia and Electrophysiology*, vol. 7, no. 5. Lippincott Williams and Wilkins, pp. 825–833, 01-Oct-2014.

[31] K. Sakata *et al.*, “Not all rotors, effective ablation targets for nonparoxysmal atrial fibrillation, are included in areas suggested by conventional indirect indicators of atrial fibrillation drivers: Extra mapping project,” *J. Arrhythmia*, vol. 34, no. 2, pp. 176–184, Apr. 2018.

[32] R. Latchamsetty and H. Oral, “Monitoring catheter ablation of AF—the European perspective,” *Nat. Rev. Cardiol. 2014 115*, vol. 11, no. 5, pp. 251–252, Mar. 2014.

[33] H. Calkins *et al.*, “2017 HRS/EHRA/ECAS/APHRS/SOLAECE expert consensus statement on catheter and surgical ablation of atrial fibrillation.”

[34] M. HAÏSSAGUERRE *et al.*, “Catheter Ablation of Chronic Atrial Fibrillation Targeting the Reinitiating Triggers,” *J. Cardiovasc. Electrophysiol.*, vol. 11, no. 1, pp. 2–10, Jan. 2000.

[35] D. P. Zipes and J. Jalife, *Cardiac Electrophysiology: From Cell to Bedside E-book: Expert Consult*. Elsevier Health Sciences, 2009.

[36] P. Jaïs *et al.*, “Technique and Results of Linear Ablation at the Mitral Isthmus,” *Circulation*, vol. 110, no. 19, pp. 2996–3002, Nov. 2004.

[37] M. Hocini *et al.*, “Techniques, Evaluation, and Consequences of Linear Block at the Left Atrial Roof in Paroxysmal Atrial Fibrillation,” *Circulation*, vol. 112, no. 24, pp. 3688–3696, Dec. 2005.

[38] A. Buttu, “Novel ECG and Intracardiac Electrograms Signal Processing Schemes for Predicting the Outcome of Atrial Fibrillation Catheter Ablation,” 2014.

[39] A. Verma *et al.*, “Approaches to Catheter Ablation for Persistent Atrial Fibrillation,” *N. Engl. J. Med.*, vol. 372, no. 19, pp. 1812–1822, May 2015.

[40] K. T. S. Konings, J. L. R. M. Smeets, O. C. Penn, H. J. J. Wellens, and M. A. Allessie, “Configuration of Unipolar Atrial Electrograms During Electrically Induced Atrial Fibrillation in Humans,” *Circulation*, vol. 95, no. 5, 1997.

[41] R. Providência *et al.*, “Is There Still a Role for Complex Fractionated Atrial Electrogram Ablation in Addition to Pulmonary Vein Isolation in Patients With Paroxysmal and Persistent Atrial Fibrillation?,” *Circ. Arrhythmia Electrophysiol.*, vol. 8, no. 5, pp. 1017–1029, Oct. 2015.

[42] S. M. Narayan, D. E. Krummen, P. Clopton, K. Shivkumar, and J. M. Miller, “Direct or coincidental elimination of stable rotors or focal sources may explain successful atrial fibrillation ablation: On-treatment analysis of the CONFIRM trial (Conventional Ablation for AF with or Without Focal Impulse and Rotor Modulation),” *J. Am. Coll. Cardiol.*, vol. 62, no. 2, pp. 138–147, Jul. 2013.

[43] P. Benharash *et al.*, “Quantitative Analysis of Localized Sources Identified by Focal Impulse and Rotor Modulation Mapping in Atrial Fibrillation,” *Circ. Arrhythmia Electrophysiol.*, vol. 8, no. 3, pp. 554–561, Jun. 2015.

[44] E. Buch *et al.*, “Long-term clinical outcomes of focal impulse and rotor modulation for treatment of atrial fibrillation: A multicenter experience,” *Hear. Rhythm*, vol. 13, no. 3, pp. 636–641, Mar. 2016.

[45] N. Tomii, K. Asano, H. Seno, T. Ashihara, I. Sakuma, and M. Yamazaki, “Validation of Intraoperative Catheter Phase Mapping Using a Simultaneous Optical Measurement System in Rabbit Ventricular Myocardium,” *Circ. J.*, p. CJ-19-1020, Mar. 2020.

[46] C. S. Elayi *et al.*, “Ablation for longstanding permanent atrial fibrillation: Results from a randomized study comparing three different strategies,” *Hear. Rhythm*, vol. 5, no. 12, pp. 1658–1664, Dec. 2008.

[47] H. Oral *et al.*, “A Randomized Assessment of the Incremental Role of Ablation of Complex Fractionated Atrial Electrograms After Antral Pulmonary Vein Isolation for Long-Lasting Persistent Atrial Fibrillation,” *J. Am. Coll. Cardiol.*, vol. 53, no. 9, pp. 782–789, Mar. 2009.

[48] A. G. Brooks *et al.*, “Outcomes of long-standing persistent atrial fibrillation ablation: A systematic review,” *Hear. Rhythm*, vol. 7, no. 6, pp. 835–846, Jun. 2010.

[49] T. Baykaner *et al.*, “Clinical Implications of Ablation of Drivers for Atrial Fibrillation: A Systematic Review and Meta-Analysis.,” *Circ. Arrhythm. Electrophysiol.*, vol. 11, no. 5, p. e006119, 2018.

[50] D. Silver *et al.*, “Mastering the game of Go with deep neural networks and tree search,” *Nature*, vol. 529, no. 7587, pp. 484–489, Jan. 2016.

[51] S. A. Abdelaziz Ismael, A. Mohammed, and H. Hefny, “An enhanced deep learning approach for brain cancer MRI images classification using residual networks,” *Artif. Intell. Med.*, vol. 102, Jan. 2020.

[52] D. Ardila *et al.*, “End-to-end lung cancer screening with three-dimensional deep learning on low-dose chest computed tomography,” *Nat. Med. 2019 256*, vol. 25, no. 6, pp. 954–961, May 2019.

[53] P. Rajan Jeyaraj and E. Rajan Samuel Nadar, “Computer-assisted medical image classification for early diagnosis of oral cancer employing deep learning algorithm,” *J. Cancer Res. Clin. Oncol.*, vol. 145, no. 3, pp. 829–837, 2019.

[54] J. Zhou *et al.*, “Weakly supervised 3D deep learning for breast cancer classification and localization of the lesions in MR images,” *J. Magn. Reson. Imaging*, vol. 50, no. 4, pp. 1144–1151, Oct. 2019.

[55] D. Zhang, S. Yang, X. Yuan, and P. Zhang, “Interpretable deep learning for automatic diagnosis of 12-lead electrocardiogram,” *iScience*, vol. 24, no. 4, Apr. 2021.

[56] R. Padmanabhan, N. Meskin, and W. M. Haddad, “Optimal adaptive control of drug dosing using integral reinforcement learning,” *Math. Biosci.*, vol. 309, pp. 131–142, Mar. 2019.

[57] M. Muffoletto, X. Fu, A. Roy, M. Varela, P. A. Bates, and O. V. Aslanidi, “Development of a Deep Learning Method to Predict Optimal Ablation Patterns for Atrial Fibrillation,” in *2019 IEEE Conference on Computational Intelligence in*

Bioinformatics and Computational Biology (CIBCB), 2019, pp. 1–4.
[58] S. Gadaleta and G. Dangelmayr, "Optimal chaos control through reinforcement learning," *Chaos An Interdiscip. J. Nonlinear Sci.*, vol. 9, no. 3, p. 775, Sep. 1999.
[59] A. L. Hodgkin and A. F. Huxley, "A quantitative description of membrane current and its application to conduction and excitation in nerve," *J. Physiol.*, vol. 117, no. 4, p. 500, 1952.
[60] C. Luo and Y. Rudy, "A model of the ventricular cardiac action potential. Depolarization, repolarization, and their interaction.," *Circ. Res.*, vol. 68, no. 6, pp. 1501–1526, 1991.
[61] M. Courtemanche, R. J. Ramirez, and S. Nattel, "Ionic mechanisms underlying human atrial action potential properties: Insights from a mathematical model," *Am. J. Physiol. - Hear. Circ. Physiol.*, vol. 275, no. 1 44-1, 1998.
[62] G. M. Faber, J. Silva, L. Livshitz, and Y. Rudy, "Kinetic properties of the cardiac L-type Ca 2+ channel and its role in myocyte electrophysiology: a theoretical investigation," *Biophys. J.*, vol. 92, no. 5, pp. 1522–1543, 2007.
[63] A. Mahajan *et al.*, "A rabbit ventricular action potential model replicating cardiac dynamics at rapid heart rates," *Biophys. J.*, vol. 94, no. 2, pp. 392–410, 2008.
[64] T. O'Hara, L. Virág, A. Varró, and Y. Rudy, "Simulation of the undiseased human cardiac ventricular action potential: model formulation and experimental validation," *PLoS Comput Biol*, vol. 7, no. 5, p. e1002061, 2011.
[65] N. A. Trayanova, R. A. Gray, D. W. Bourn, and J. C. Eason, "Virtual Electrode-Induced Positive and Negative Graded Responses:," *J. Cardiovasc. Electrophysiol.*, vol. 14, no. 7, pp. 756–763, Jul. 2003.
[66] T. Ashihara, T. Namba, M. Ito, T. Ikeda, K. Nakazawa, and N. Trayanova, "Spiral Wave Control by a Localized Stimulus: A Bidomain Model Study," *J. Cardiovasc. Electrophysiol.*, vol. 15, no. 2, pp. 226–233, Feb. 2004.
[67] T. Ashihara and N. A. Trayanova, "Asymmetry in membrane responses to electric shocks: insights from bidomain simulations," *Biophys. J.*, vol. 87, no. 4, pp. 2271–2282, 2004.
[68] K. SKOUIBINE, N. TRAYANOVA, and P. MOORE, "Success and Failure of the Defibrillation Shock:," *J. Cardiovasc. Electrophysiol.*, vol. 11, no. 7, pp. 785–796, Jul. 2000.
[69] O. Ronneberger, P. Fischer, and T. Brox, "U-net: Convolutional networks for biomedical image segmentation," in *Lecture Notes in Computer Science (including subseries Lecture Notes in Artificial Intelligence and Lecture Notes in Bioinformatics)*, 2015, vol. 9351, pp. 234–241.
[70] A. Paszke *et al.*, "Automatic differentiation in PyTorch," Oct. 2017.
[71] J. A. B. Zaman, N. S. Peters, and S. M. Narayan, "Rotor mapping and ablation to treat atrial fibrillation," *Current Opinion in Cardiology*, vol. 30, no. 1. Lippincott Williams and Wilkins, pp. 24–32, 12-Jan-2015.

[72] N. Tomii, M. Yamazaki, T. Arafune, H. Honjo, N. Shibata, and I. Sakuma, “Detection Algorithm of Phase Singularity Using Phase Variance Analysis for Epicardial Optical Mapping Data,” *IEEE Trans. Biomed. Eng.*, vol. 63, no. 9, pp. 1795–1803, Sep. 2016.

[73] N. Tomii *et al.*, “Interaction of phase singularities on the spiral wave tail: reconsideration of capturing the excitable gap,” *Am. J. Physiol. Circ. Physiol.*, vol. 315, no. 2, pp. H318–H326, Aug. 2018.

[74] J. M. Davidenko, R. Salomonsz, A. M. Pertsov, W. T. Baxter, and J. Jalife, “Effects of pacing on stationary reentrant activity theoretical and experimental study,” *Circ. Res.*, vol. 77, no. 6, pp. 1166–1179, Dec. 1995.

[75] C. M. Augustin *et al.*, “The impact of wall thickness and curvature on wall stress in patient-specific electromechanical models of the left atrium,” *Biomech. Model. Mechanobiol.*, vol. 19, no. 3, pp. 1015–1034, Jun. 2020.

[76] J. S. Song *et al.*, “Pro-arrhythmogenic effects of heterogeneous tissue curvature ― A suggestion for role of left atrial appendage in atrial fibrillation ―,” *Circ. J.*, vol. 83, no. 1, pp. 32–40, Dec. 2019.

[77] K. Tanaka *et al.*, “Spatial distribution of fibrosis governs fibrillation wave dynamics in the posterior left atrium during heart failure,” *Circ. Res.*, vol. 101, no. 8, pp. 839–847, Oct. 2007.

[78] S. Nattel, B. Burstein, and D. Dobrev, “Atrial remodeling and atrial fibrillation: mechanisms and implications.,” *Circ. Arrhythm. Electrophysiol.*, vol. 1, no. 1, pp. 62–73, Apr. 2008.

[79] D. J. Gauthier, G. M. Hall, R. A. Oliver, E. G. Dixon-Tulloch, P. D. Wolf, and S. Bahar, “Progress toward controlling in vivo fibrillating sheep atria using a nonlinear-dynamics-based closed-loop feedback method,” *Chaos An Interdiscip. J. Nonlinear Sci.*, vol. 12, no. 3, p. 952, Aug. 2002.

[80] M. M. Refaat *et al.*, “Swine atrioventricular node ablation using stereotactic radiosurgery: Methods and in vivo feasibility investigation for catheter-free ablation of cardiac arrhythmias,” *J. Am. Heart Assoc.*, vol. 6, no. 11, Nov. 2017.